NATURE NEUROSCIENCE | ARTICLE

A common haplotype lowers PU.1 expression in myeloid cells and delays onset of Alzheimer's disease

Kuan-lin Huang,, Edoardo Marcora,, Anna A Pimenova,, Antonio F Di Narzo,, Manav Kapoor,, Sheng Chih Jin,, Oscar Harari,, Sarah Bertelsen,, Benjamin P Fairfax,, Jake Czajkowski,, Vincent Chouraki,, Benjamin Grenier-Boley,, Céline Bellenguez,, Yuetiva Deming,, Andrew McKenzie,, Towfique Raj,, Alan E Renton,, John Budde,, Albert Smith,, Annette Fitzpatrick,, Joshua C Bis,, Anita DeStefano,, Hieab H H Adams,, M Arfan Ikram,, Sven van der Lee *et al.*

Nature Neuroscience (2017) doi:10.1038/nn.4587
Received 30 June 2016 Accepted 20 May 2017 Published online 19 June 2017

Abstract

A genome-wide survival analysis of 14,406 Alzheimer's disease (AD) cases and 25,849 controls identified eight previously reported AD risk loci and 14 novel loci associated with age at onset. Linkage disequilibrium score regression of 220 cell types implicated the regulation of myeloid gene expression in AD risk. The minor allele of rs1057233 (G), within the previously reported *CELF1* AD risk locus, showed association with delayed AD onset and lower expression of *SPI1* in monocytes and macrophages. *SPI1* encodes PU.1, a transcription factor critical for myeloid cell development and function. AD heritability was enriched within the PU.1 cistrome, implicating a myeloid PU.1 target gene network in AD. Finally, experimentally altered PU.1 levels affected the expression of mouse orthologs of many AD risk genes and the phagocytic activity of mouse microglial cells. Our results suggest that lower *SPI1* expression reduces AD risk by regulating myeloid gene expression and cell function.

Subject terms: Data integration Genome-wide association studies Neurodegenerative diseases

Introduction

AD is the most prevalent form of dementia. While genome-wide association studies (GWAS) have identified more than twenty AD risk loci[1, 2, 3, 4, 5], the associated disease genes and mechanisms remain largely unclear. To better understand these genetic associations, AD-related phenotypes can be leveraged. For example, few studies[6, 7] have investigated the genetic basis of age at onset of AD (AAO). To date, *APOE* remains the only locus repeatedly associated with AAO[8, 9], but *PICALM* and *BIN1* have also been reported to affect AAO[6, 10, 11]. Further, we have previously used cerebrospinal fluid (CSF) biomarkers to demonstrate that *APOE* genotype is strongly associated with these disease-relevant endophenotypes[12, 13].

Identifying causal genes and mechanisms underlying disease-associated loci requires integrative analyses of expression and epigenetic datasets in disease-relevant cell types[14]. Recent genetic and molecular evidence has highlighted the role of myeloid cells in AD pathogenesis. At the genetic level, GWAS and sequencing studies have found associations between AD and genes expressed in myeloid cells, including *TREM2*, *ABCA7* and *CD33*[1, 2, 5, 15, 16, 17]. At the epigenetic level, genes expressed in myeloid cells display abnormal patterns of chromatin modification in AD mouse models and human samples[18, 19, 20]. Further, AD-risk alleles are polarized for *cis*-expression quantitative trait locus (*cis*-eQTL) effects in monocytes[21]. Here we show that AD heritability is enriched in functional annotations for cells of the myeloid and B-lymphoid lineage, suggesting that integrative analyses of AD loci with myeloid-specific expression and

epigenetic datasets will uncover novel AD genes and mechanisms related to the function of these cell types.

In this study, we conducted a large-scale genome-wide survival analysis and subsequent endophenotype association analysis to uncover loci associated with AAO-defined survival (AAOS) in AD cases and nondemented elderly controls. We discovered an AAOS- and CSF $A\beta_{42}$-associated single nucleotide polymorphism (SNP), rs1057233, in the previously reported *CELF1* AD risk locus. *Cis*-eQTL analyses revealed a highly significant association of the protective rs1057233^{G} allele with reduced *SPI1* expression in human myeloid cells. *SPI1* encodes PU.1, a transcription factor critical for myeloid and B-lymphoid cell development and function, which binds to the *cis*-regulatory elements of several AD-associated genes in these cells. Moreover, we show that AD heritability was enriched in PU.1 ChIP-seq binding sites in human myeloid cells across the genome, implicating a myeloid PU.1 target gene network in the etiology of AD. To validate these bioinformatic analyses, we show that experimentally altered PU.1 levels correlated with phagocytic activity of mouse microglial cells and the expression of multiple genes involved in diverse biological processes of myeloid cells. This evidence collectively shows that lower *SPI1* expression may reduce AD risk by modulating myeloid cell gene expression and function.

Results

Genome-wide survival analysis

For the genome-wide survival analysis, we used 14,406 AD case samples and 25,849 control samples from the International Genomics of Alzheimer's Project (IGAP) consortium (Table 1a). Of these, 8,253,925 SNPs passed quality control and were included for meta-analysis across all cohorts (Supplementary Table 1), which showed little evidence of genomic inflation ($\lambda = 1.026$). Four loci showed genome-wide significant associations ($P < 5 \times 10^{-8}$) with AAOS: *BIN1* ($P = 3.9 \times 10^{-10}$), *MS4A* ($P = 2.3 \times 10^{-9}$), *PICALM* ($P = 9.1 \times 10^{-12}$) and *APOE* ($P = 7.8 \times 10^{-52}$) Supplementary Fig. 1). While SNPs within *BIN1*[6], *PICALM*[6, 10] and *APOE*[6, 8, 9, 10] loci have previously been shown to be associated with AAO, to our knowledge this is the first time the *MS4A* locus has been reported to be associated with an AAO-related phenotype. The minor allele of rs7930318 near *MS4A4A* was associated with delayed AAO. Four other AD risk loci previously reported in the IGAP GWAS[1] showed associations that reached suggestive significance ($P < 1.0 \times 10^{-5}$): *CR1* ($P = 1.2 \times 10^{-6}$), *SPI1* (previously labeled as *CELF1* in the 2013 IGAP GWAS paper[1]; $P = 8.4 \times 10^{-6}$), *SORL1* ($P = 5.5 \times 10^{-6}$) and *FERMT2* ($P = 2.3 \times 10^{-6}$). The direction of effects was concordant with the previous IGAP GWAS logistic regression analysis for AD risk[1] at all suggestive loci: AD risk-increasing alleles were all associated with a hazard ratio above 1 and earlier AAO, whereas AD risk-decreasing alleles were all associated with a hazard ratio below 1 and later AAO (Table 1b and Supplementary Table 2). We also identified 14 loci that reached suggestive significance in the survival analysis, three of which (rs116341973, rs1625716 and rs11074412) were nominally associated with AD risk (Bonferroni-corrected threshold: $P = 0.05/22 = 2.27 \times 10^{-3}$) in the IGAP GWAS (Table 1b and Supplementary Figs. 2 and 3).

Table 1: Genome-wide survival analysis of Alzheimer's disease

Cerebrospinal fluid biomarkers associations

To further validate the 22 loci with at least suggestive associations to AAOS, we examined their associations with CSF biomarkers, including total tau, phosphorylated tau_{181} and $A\beta_{42}$ in a dataset of 3,646 Caucasians extended from our previous report[12] (Table 2). Two SNPs showed associations that reached the Bonferroni-corrected threshold ($P < 2.27 \times 10^{-3}$). Rs4803758, near *APOE*, showed the most significant associations with levels of CSF phosphorylated tau_{181} ($P = 3.75 \times 10^{-4}$) and CSF $A\beta_{42}$ ($P = 3.12 \times 10^{-5}$), whereas rs1057233, in the *SPI1* locus, was significantly associated with CSF $A\beta_{42}$ ($P = 8.24 \times 10^{-4}$). Of note, a SNP adjacent to *VLDLR*, rs7867518, showed the most significant association with CSF total tau ($P = 5.83 \times 10^{-3}$) but failed to pass the Bonferroni-corrected threshold. The protective and deleterious effects in the survival analysis of these three SNPs were concordant with directionalities of their CSF biomarker associations; for example, the protective rs1057233^{G} allele was associated with higher CSF $A\beta_{42}$ levels and the risk rs1057233^{A} allele was associated with lower CSF $A\beta_{42}$ levels.

Table 2: Summary of CSF-biomarker associations of suggestive and significant AAOS-associated SNPs

Cis-eQTL associations and colocalization analysis

Multiple disease-associated GWAS SNPs have been identified as *cis*-eQTLs of disease genes in disease-relevant tissues and/or cell types[22]. We investigated *cis*-eQTL effects of the 22 AAOS-associated SNPs and their tagging SNPs ($R^2 \geq 0.8$; Supplementary Table 3) in the BRAINEAC dataset (see URLs). We identified four significant associations (Bonferroni-corrected threshold: $P = 0.05/292{,}000$ probes = 1.7×10^{-7}): rs1057233 was associated with *MTCH2* expression in the cerebellum ($P = 1.20 \times 10^{-9}$); rs7445192 was associated with *SRA1*

expression (averaged across brain regions, $P = 7.0 \times 10^{-9}$, or in the frontal cortex, $P = 1.6 \times 10^{-7}$, for two different probes) and rs2093761 was associated with *CR1* and *CR1L* expression in white matter ($P = 1.30 \times 10^{-7}$; Supplementary Table 4). Further analysis using the GTEx dataset[23] identified 50 unique, associated SNP–gene pairs across 44 tissues, including 11 SNP–gene pairs in various brain regions (Supplementary Table 5).

Recently, genetic and molecular evidence has implicated myeloid cells in the etiology of AD, including our finding that AD risk alleles are enriched for *cis*-eQTL effects in $CD14^+$ monocytes but not in $CD4^+$ T-lymphocytes[21]. To extend this finding and identify relevant cell types in AD, we used stratified linkage disequilibrium (LD) score regression to estimate enrichment of AD heritability (as measured by summary statistics from IGAP GWAS[1]) partitioned by 220 cell-type-specific functional annotations as described by Finucane *et al*.[24]. We found a significant enrichment of AD heritability in hematopoietic cells of the myeloid and B-lymphoid lineage (for example, 14.49-fold enrichment, $P = 3.49 \times 10^{-5}$, in H3K4me1-tagged enhancers of $CD14^+$ monocytes; and 12.33-fold enrichment, $P = 1.41 \times 10^{-6}$, in H3K4me1-tagged enhancers of $CD19^+$ B cells). In contrast, schizophrenia heritability was not enriched in hematopoietic cells (1.24-fold enrichment, $P = 0.53$, as measured by summary statistics from the Psychiatric Genomics Consortium GWAS[25]) but was significantly enriched in brain (18.61-fold enrichment, $P = 1.38 \times 10^{-4}$, in H3K4me3-tagged promoters of fetal brain; Supplementary Table 6). These results suggest that myeloid cells specifically modulate AD susceptibility.

Based on these observations, we hypothesized that *cis*-eQTL effects of some AD-associated alleles may be specific to myeloid cells and thus not easily detectable in *cis*-eQTL datasets obtained from brain homogenates where myeloid cells (microglia and other brain-resident macrophages) represent a minor fraction of the tissue. Therefore, we analyzed *cis*-eQTL effects of the AAOS-associated SNPs and their tagging SNPs in human *cis*-eQTL datasets composed of 738 monocyte and 593 macrophage samples from the Cardiogenics consortium[26]. We identified 14 genes with *cis*-eQTLs significantly associated with these SNPs (Table 3). Notably, the protective $rs1057233^G$ allele, located within the 3′ untranslated region (UTR) of *SPI1*, was strongly associated with lower expression of *SPI1* in both monocytes ($P = 1.50 \times 10^{-105}$) and macrophages ($P = 6.41 \times 10^{-87}$; Figs. 1a,b and 2a). This allele was also associated with lower expression of *MYBPC3* in both monocytes ($P = 4.99 \times 10^{-51}$) and macrophages ($P = 5.58 \times 10^{-23}$), higher expression of *CELF1* in monocytes ($P = 3.95 \times 10^{-8}$) and lower expression of *NUP160* in macrophages ($P = 5.35 \times 10^{-22}$). Each of these genes lies within the *SPI1* locus, suggesting complex regulation of gene expression in this region. Within the *MS4A* locus, which contains many gene family members, the minor allele (C) of rs7930318 was consistently associated with lower expression of *MS4A4A* in monocytes ($P = 8.20 \times 10^{-28}$) and *MS4A6A* in both monocytes ($P = 4.90 \times 10^{-23}$) and macrophages ($P = 1.25 \times 10^{-9}$; Fig. 1b).

Table 3: Significant *cis*-eQTL associations of the 22 suggestive and significant AAOS-associated SNPs

Figure 1: AD-survival and myeloid eQTL associations.

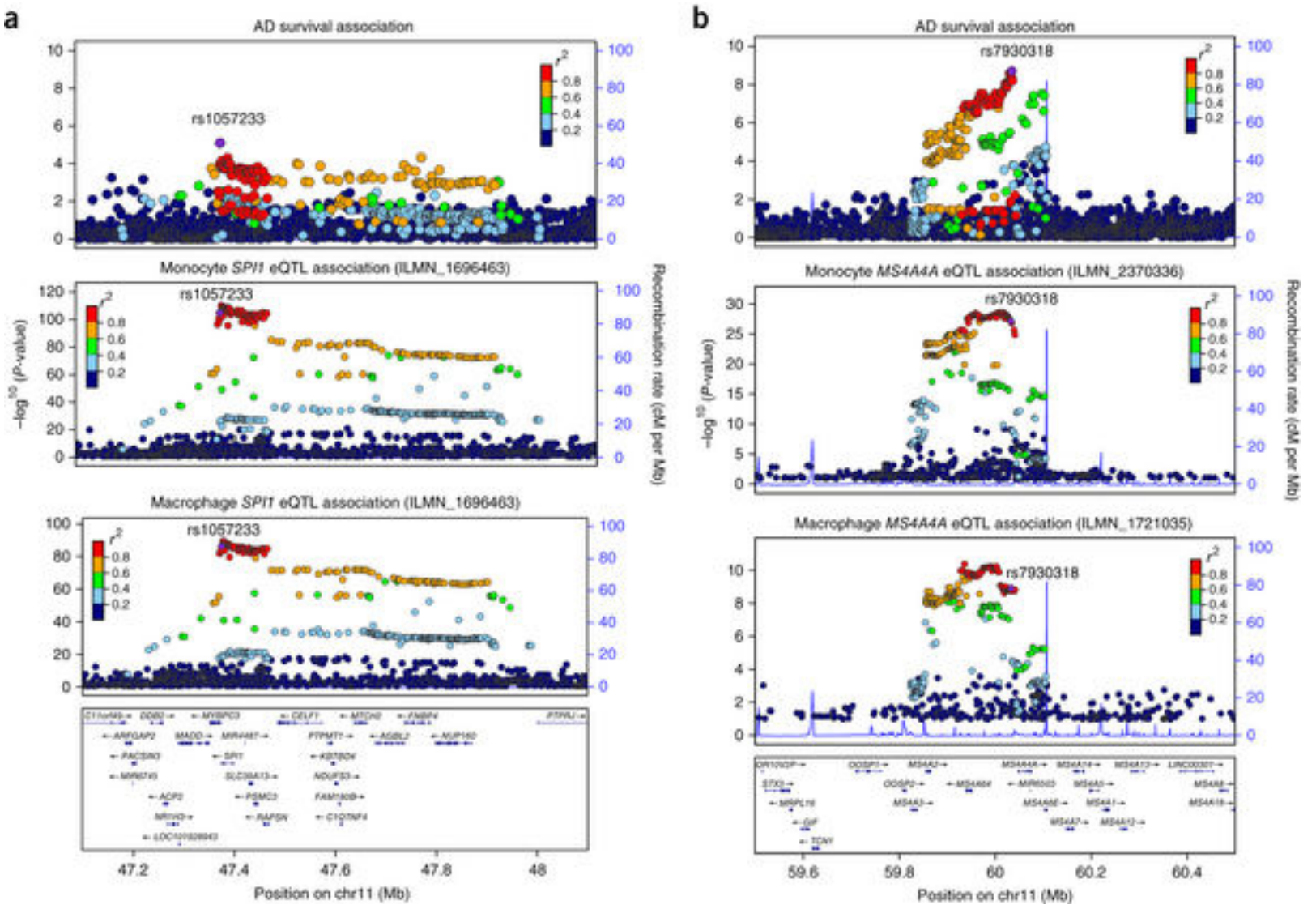

(**a**) The AD-survival association landscape at the *SPI1* locus resembles that of *SPI1 cis*-eQTL association in monocytes and macrophages. (**b**) The AD-survival association landscape at the *MS4A* locus resembles that of *MS4A4A* and *MS4A6A cis*-eQTL association in monocytes and macrophages. Chr11, chromosome 11.

Figure 2: *SPI1* (PU.1) expression and ChIP-seq analysis.

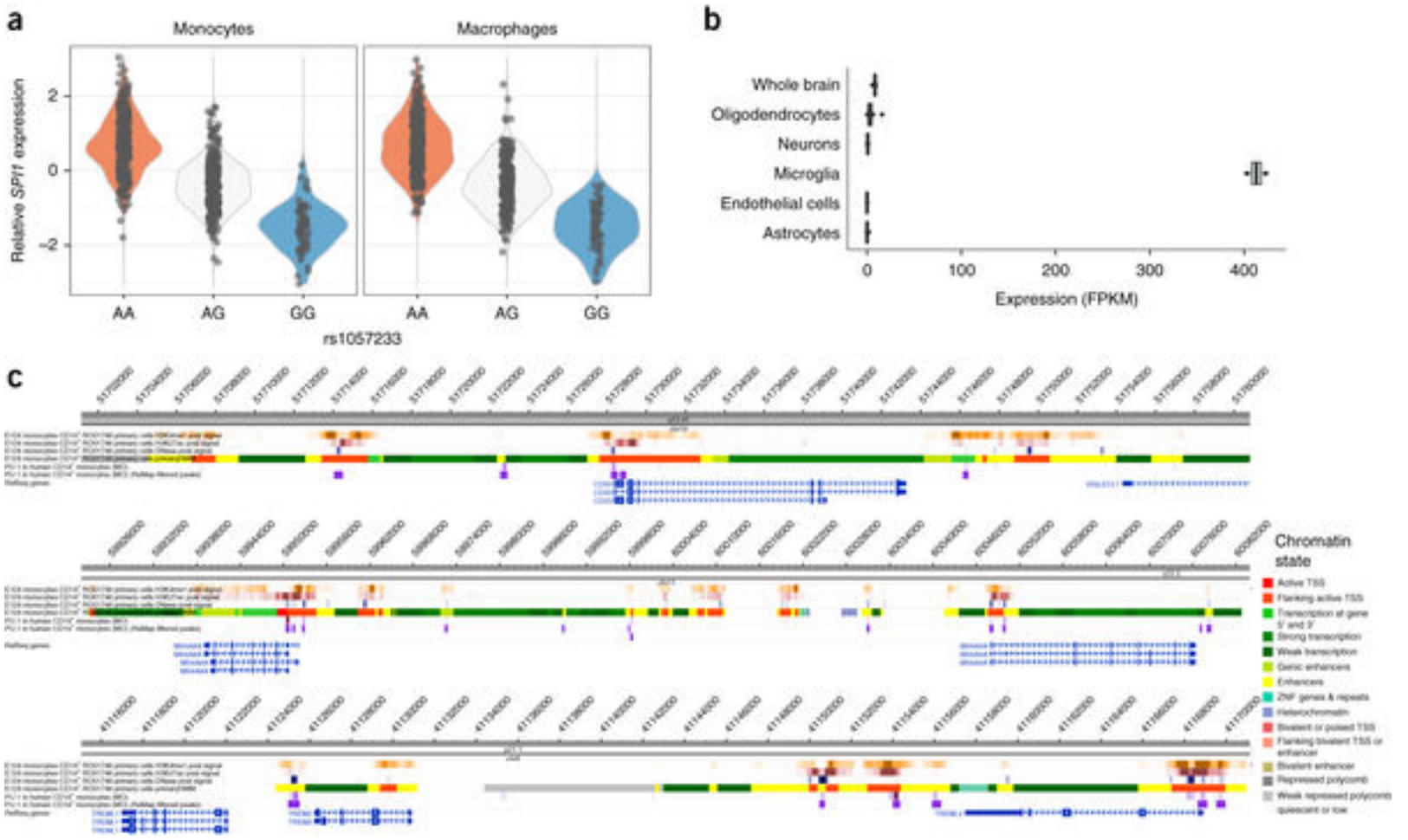

(**a**) Rs1057233^{G} is associated with reduced *SPI1* expression in a dosage-dependent manner. (**b**) The mouse homolog of *SPI1*, *Sfpi1* or *Spi1*, is selectively expressed in microglia and macrophages in mouse brains based on the brain RNA-seq database[28, 29, 30]. Oligodendrocyte precursor cells (OPCs) contain 5% microglial contamination. (**c**) 1) binds to the promoter and regulatory regions of *CD33*, *MS4A4A*, *MS4A6A*, *TREM2* and *TREML2* in human CD14^{+} monocytes, based on ChIP-seq data[34]. ZNF, zinc finger; TSS, transcription start site.

We then sought evidence of replication in an independent dataset of primary CD14^{+} human monocytes from 432 individuals[27]. We replicated *cis*-eQTL associations with expression of *SPI1*, *MYBPC3*, *MS4A4A*, *MS4A6A* and *SELL* (Bonferroni-corrected threshold: *P* =

0.05/15,421 probes = 3.24×10^{-6}). We found strong evidence for the association between rs1057233 and *SPI1* expression ($P = 6.39 \times 10^{-102}$) as well as *MYBPC3* expression ($P = 5.95 \times 10^{-33}$; Supplementary Table 7). Rs1530914 and rs7929589, both in high LD with rs7930318 ($R^2 = 0.99$ and 0.87, respectively), were associated with expression of *MS4A4A* ($P = 3.60 \times 10^{-8}$) and *MS4A6A* ($P = 6.37 \times 10^{-15}$). Finally, rs2272918, tagging rs10919252, was significantly associated with expression of *SELL* ($P = 8.43 \times 10^{-16}$). Notably, the minor alleles of all of these SNPs showed protective effects in both AD risk and survival analyses, as well as lower expression of the associated genes. Further, based on RNA-seq data *SPI1*, *MS4A4A*, *MS4A6A* and *SELL* are specifically expressed in microglia[28, 29, 30] (Fig. 2b and Supplementary Fig. 4). However, *MYBPC3*, which produces Mybpc3 (a myosin binding protein expressed at high levels in cardiac muscle cells), is either not expressed or expressed at low levels in human and mouse microglia, respectively. Amongst all genes probed, *MYBPC3* (ILMN_1781184) expression was the most highly and significantly correlated with *SPI1* (ILMN_1696463) expression in both Cardiogenics datasets (Spearman's $\rho = 0.54$, qval = 0.00 in monocytes; Spearman's $\rho = 0.42$, qval = 0.00 in macrophages), suggesting that low levels of *MYBPC3* expression in human myeloid cells are possibly due to leaky transcription driven by the adjacent highly expressed *SPI1* gene.

We performed the coloc test[31] to determine whether AAOS-associated SNPs co-localize with myeloid *cis*-eQTLs at the *SPI1*, *MS4A* and *SELL* loci. These analyses (Supplementary Table 8) highlighted *SPI1* at the *SPI1* locus as the strongest and most consistent colocalization target and the only gene in which AD survival and gene expression association signals are likely (posterior probability ≥ 0.8) driven by the same causal genetic variant, in both monocytes and macrophages (PP.H4.abf values of 0.85 and 0.83, respectively). *MYBPC3* in the *SPI1* locus and *MS4A6A* in the *MS4A* locus each also showed evidence of colocalization in both myeloid cell types but did not reach the posterior probability cutoff in one cell type each (*MYBPC3* failed to reach the cutoff in monocytes and *MS4A6A* failed to reach the cutoff in macrophages). *MS4A4A* and *MS4A6E* in the *MS4A* locus showed evidence of co-localization only in monocytes, while *SELL* did not show evidence of colocalization. In light of the strong *cis*-eQTL effects and colocalization results described above, we decided to focus subsequent analyses on *SPI1* as the strongest candidate gene underlying the disease association in myeloid cells.

Conditional and SMR analysis of the *SPI1* locus

The AAOS-association landscape shows that highly associated SNPs at the *SPI1* locus span multiple genes (Fig. 1a). In the previous IGAP GWAS[1], rs10838725 showed the strongest association at this locus ($P = 6.7 \times 10^{-6}$ and $P = 1.1 \times 10^{-8}$ versus rs1057233: $P = 5.4 \times 10^{-6}$ and $P = 5.9 \times 10^{-7}$ in IGAP stage I and in IGAP stages I and II combined, respectively). Rs10838725 is located in the intron of *CELF1*, which was assigned as the putative causal gene at this locus[1] based on its proximity to the index SNP, a criterion that has often proven to be erroneous[14]. In our survival analysis, however, rs10838725 showed weak association ($P = 0.12$, Hazard Ratio (HR) = 1.02, 95% confidence interval (CI) = 0.99–1.05), whereas rs1057233, located in the 3′ UTR of a neighboring gene, *SPI1*, showed the strongest association (Table 1; $P = 8.4 \times 10^{-6}$, HR = 0.94, CI = 0.91–0.97). The two SNPs exhibit only moderate LD in the Alzheimer's Disease Genetics Consortium (ADGC) subset of the IGAP GWAS ($R^2 = 0.21$, $D' = 0.96$). Applying conditional logistic regression analysis of AD risk in the ADGC dataset, we found that rs1057233 remained significantly associated with AD after adjusting for rs10838725 ($P = 3.2 \times 10^{-4}$), whereas rs10838725 showed no evidence of association after adjusting for rs1057233 ($P = 0.66$). This suggests that rs1057233 is in stronger LD with the AD risk causal variant.

The association landscape in the AD survival analysis strongly resembles that of *SPI1 cis*-eQTL analysis in myeloid cells (Fig. 1a). We reasoned that the associations of rs1057233 with AD-related phenotypes may be explained by the regulation of *SPI1* expression in myeloid cells and that conditional analysis of the *cis*-eQTL signal could help us further dissect this complex locus. Therefore, we conducted conditional *cis*-eQTL analyses in both Cardiogenics datasets as we did above using rs1057233 (the top SNP for AD survival) and rs10838725 (the top SNP for AD risk). In addition, we also examined rs10838698 (an SNP in high LD with rs1057233 that was directly genotyped in the Cardiogenics dataset) and rs1377416, a SNP in high LD with rs10838725, which is proposed as a functional variant in an enhancer near *SPI1* that is active in human myeloid cells and in the brain of a mouse model of AD[19]. It should be noted that rs1057233 is a functional variant that has been shown to directly affect *SPI1* expression by changing the target sequence and binding of the microRNA miR-569[32]. Rs1057233 and rs10838698 remained significantly associated with *SPI1* expression when adjusting for either of the other two SNPs in both monocytes and macrophages ($P < 8.33 \times 10^{-3}$). However, conditioning for either of these two SNPs abolished the associations of rs1377416 and rs10838725 with *SPI1* expression (Supplementary Table 9). Thus, the functional variant(s) mediating the effect on *SPI1* expression and AD risk likely reside(s) in the LD block that includes rs1057233 and rs10838698 but not rs10838725 and rs1377416 (Supplementary Fig. 5).

Using HaploReg[33] to annotate the top AAOS-associated SNP (rs1057233) and its tagging SNPs ($R^2 \geq 0.8$; Supplementary Table 3), we

identified multiple SNPs (for example, rs10838699 and rs7928163) in high LD with rs1057233 that changed the predicted DNA-binding motif of *SPI1* (PU.1), raising the possibility of altered self-regulation associated with the minor allele. Based on these results, one or more of these or other SNPs in very high LD with rs1057233 could explain the observed associations with *SPI1* expression and AD-related phenotypes.

We also conducted summary-databased Mendelian randomization (SMR) and heterogeneity in dependent instruments (HEIDI) tests[22] to prioritize likely causal genes and variants by integrating summary statistics from our AAOS GWAS and the Cardiogenics study (Supplementary Table 10). SMR–HEIDI analysis was performed for the *SPI1* locus, using rs1057233, rs10838698, rs10838699, rs7928163, rs10838725 and rs1377416 as candidate causal variants. In both monocytes and macrophages, *SPI1* was consistently identified as the most likely gene whose expression levels were associated with AD survival because of causality or pleiotropy at the same underlying causal variant (rs1057233, rs10838698, rs10838699 or rs7928163 in the same LD block; SMR, $P < 4.90 \times 10^{-4}$, Bonferroni-corrected threshold for $n = 6$ SNPs tested against 17 probes and HEIDI, $P \geq 0.05$; Supplementary Fig. 6). Neither conditional analysis nor SMR–HEIDI analyses could definitively identify a single functional variant among this set of four SNPs in high LD. Functional analyses will be necessary to determine which SNPs in this LD block directly affect *SPI1* expression. Overall, rs1057233 and tagging SNPs are associated with AD risk and survival and with CSF $A\beta_{42}$. The strong *cis*-eQTL effects and colocalization results point to *SPI1* as the most likely candidate gene underlying the disease association at the *SPI1* locus.

SPI1 (PU.1) cistrome and functional analysis in myeloid cells

SPI1 encodes PU.1, a transcription factor essential for the development and function of myeloid cells. We hypothesize that it may modulate AD risk by regulating the transcription of AD-associated genes expressed in microglia and/or in other myeloid cell types. First, we tested AD-associated genes for evidence of expression in human microglia[28] as well as presence of PU.1 binding peaks in *cis*-regulatory elements of these genes using ChIP-seq datasets obtained from human monocytes and macrophages[34]. We specifically investigated 112 AD-associated genes, including the 104 genes located within IGAP GWAS loci[35] plus *APOE*, *APP*, *TREM2* and *TREML2, TYROBP*, *TRIP4*, *CD33*, and *PLD3*. Of these genes, 75 had evidence of gene expression in human brain microglial cells, 60 of which also had evidence of association with PU.1 binding sites in human blood myeloid cells[34] (Supplementary Table 11). Further examination of PU.1 binding peaks and chromatin marks or states in human monocytes confirmed that PU.1 is bound to *cis*-regulatory elements of many AD-associated genes, including *ABCA7*, *CD33*, *MS4A4A*, *MS4A6A*, *PILRA*, *PILRB*, *TREM2*, *TREML2* and *TYROBP* (as well as *SPI1* itself but, notably, not *APOE*; Fig. 2c and Supplementary Fig. 7). Together, these results suggest that PU.1 may regulate the expression of multiple AD-associated genes in myeloid cells.

To further support the hypothesis that PU.1 target genes expressed in myeloid cells may be associated with AD risk, we used stratified LD score regression[24] to estimate the enrichment of AD heritability (as measured by summary statistics from the IGAP GWAS[1]) partitioned on the PU.1 cistrome, as profiled by ChIP-seq in human monocytes and macrophages[34]. We found a significant enrichment of AD heritability in both monocytes (47.58-fold enrichment, $P = 6.94 \times 10^{-3}$) and macrophages (53.88-fold enrichment, $P = 1.65 \times 10^{-3}$) but not of schizophrenia heritability (as measured by summary statistics from the Psychiatric Genomics Consortium GWAS[25]; Supplementary Table 12). Thus, the contribution of the myeloid PU.1 target gene network to disease susceptibility is specific to AD. However, since PU.1 is a key myeloid transcription factor that regulates the expression of a large number of genes in myeloid cells, the enrichment of AD risk alleles in PU.1 binding sites could simply reflect an enrichment of AD GWAS associations for genes that are expressed in myeloid cells rather than specifically among PU.1 target genes. To attempt to address this issue, we performed stratified LD score regression of AD heritability partitioned by functional annotations obtained from *SPI1* (marking the PU.1 cistrome) and POLR2AphosphoS5 (marking actively transcribed genes) ChIP-seq experiments, performed in duplicate, using a human myeloid cell line (HL60) by the ENCODE Consortium[36]. We observed a significant enrichment for *SPI1* (PU.1; 34.58-fold enrichment, $P = 1.31 \times 10^{-3}$, in the first replicate; 58.12-fold enrichment, $P = 4.95 \times 10^{-3}$, in the second replicate), much stronger than that for POLR2AphosphoS5 (15.78-fold enrichment, $P = 1.71 \times 10^{-2}$, in the first replicate; 16.34-fold enrichment, $P = 1.25 \times 10^{-1}$, in the second replicate), consistent with our hypothesis (Supplementary Table 12).

PU.1 target genes are implicated in various biological processes of myeloid cells that may modulate AD risk. For example, a microglial gene network for pathogen phagocytosis has been previously implicated in the etiology of AD[18]. We modulated levels of PU.1 by *Spi1* cDNA overexpression or shRNA knockdown in BV2 mouse microglial cells and used zymosan bioparticles labeled with pHrodo (a pH-sensitive dye that emits a fluorescent signal when internalized in acidic vesicles during phagocytosis) to measure pathogen engulfment. Analysis of zymosan uptake by flow cytometry revealed that phagocytic activity is augmented in BV2 cells overexpressing PU.1 (Fig. 3a), while knockdown of PU.1 resulted in decreased phagocytic activity (Fig. 3a). We confirmed overexpression and knockdown of PU.1 expression

levels by western blotting and quantitative PCR (qPCR; Figs. 3b–d and 4a). Phagocytic activity was not changed in untransfected cells when analyzed by flow cytometry (Supplementary Fig. 8d–g). These data suggest that modulation of PU.1 expression levels significantly changes microglial phagocytic activity in response to fungal targets (mimicked by zymosan; $P = 0.0295$ for overexpression and $P = 0.001$ for knockdown of PU.1; Fig. 3).

Figure 3: PU.1 modulates the phagocytic activity of BV2 microglial cells.

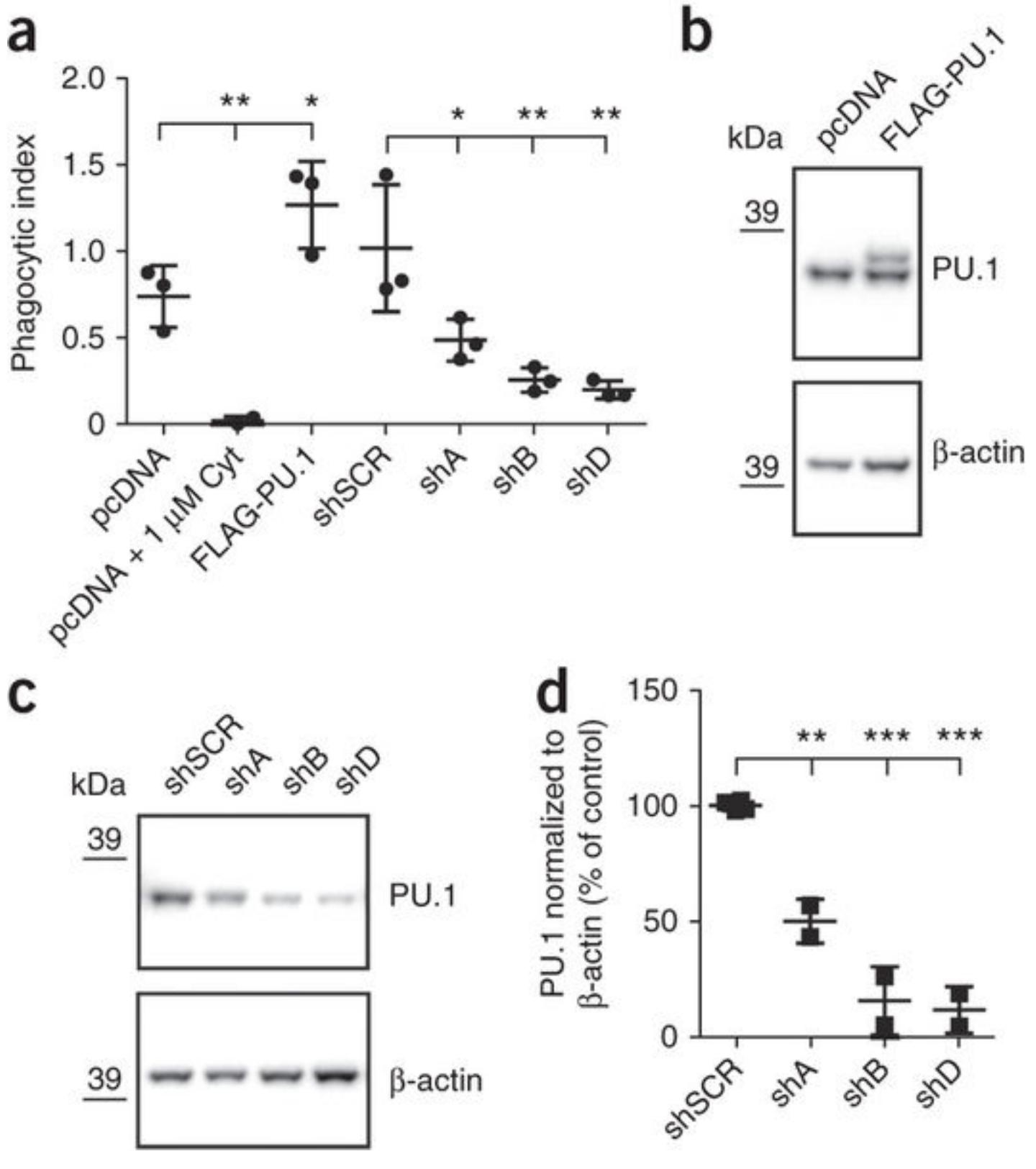

(**a**) Phagocytosis of zymosan labeled with red pHrodo fluorescent dye in BV2 cells with transient overexpression (FLAG-1, FLAG peptide-tagged 1 in a pcDNA3 vector; pcDNA, empty pcDNA3 vector as a control) and knockdown of 1 (shA, shB and shD are shRNA targeting 1; shSCR is a scrambled shRNA used as a control) was measured by flow cytometry. Cytochalasin D (Cyt) treatment was used as a negative control. Mean phagocytic index ± s.d. is shown: pcDNA, 0.7373 ± 0.1772; pcDNA + 1 μM Cyt, 0.0236 ± 0.0242; FLAG-1 1.2630 ± 0.2503; shSCR, 1.014 ± 0.3656; shA 0.4854 ± 0.1209; shB, 0.2579 ± 0.06967; shD 0.2002 ± 0.05168 ($F_{6,13} = 14.82$; pcDNA vs. pcDNA + 1 μM Cyt, $P = 0.0078$; pcDNA vs. FLAG-1, $P = 0.0295$; shSCR vs. shA, $P = 0.0283$; shSCR vs. shB, $P = 0.0020$; shSCR vs. shD, $P = 0.0010$; $n = 3$). (**b**) BV2 cells were transiently transfected with pcDNA3 (pcDNA) or pcDNA3-FLAG-1 (FLAG-1) and pCMV-GFP, a vector expressing GFP as described for phagocytosis assay. Note a shift in mobility of the band for exogenous FLAG-1 in the overexpression condition compared to endogenous 1 in controls. (**c**) BV2 cells were transiently transfected with shRNA targeting 1 (shA, shB and shD) or nontargeting control shRNA (shSCR) in the pGFP-V-RS vector backbone. GFP^+ cells were sorted by flow cytometry and analyzed for levels of 1 in western blotting in two independent experiments (**b** and **c**). (**d**) Quantification of 1 levels in **c** normalized to β-actin as a loading control. Values are presented as mean ± s.d.: shSCR, 100 ± 2.10; shA, 50.34 ± 9.52; shB, 16.03 ± 14.72; shD, 12.13 ± 10.03 ($F_{3,6} = 70.55$; shSCR vs. shA, $P = 0.0014$; shSCR vs. shB, $P < 0.0001$; shSCR vs. shD, $P < 0.0001$; $n = 2$). *$P < 0.05$, **$P < 0.01$, ***$P < 0.001$; one-way ANOVA with Sidak's *post hoc* multiple comparisons test between selected groups.

Figure 4: Genes regulated with differential expression of *Spi1* in BV2 microglial cells.

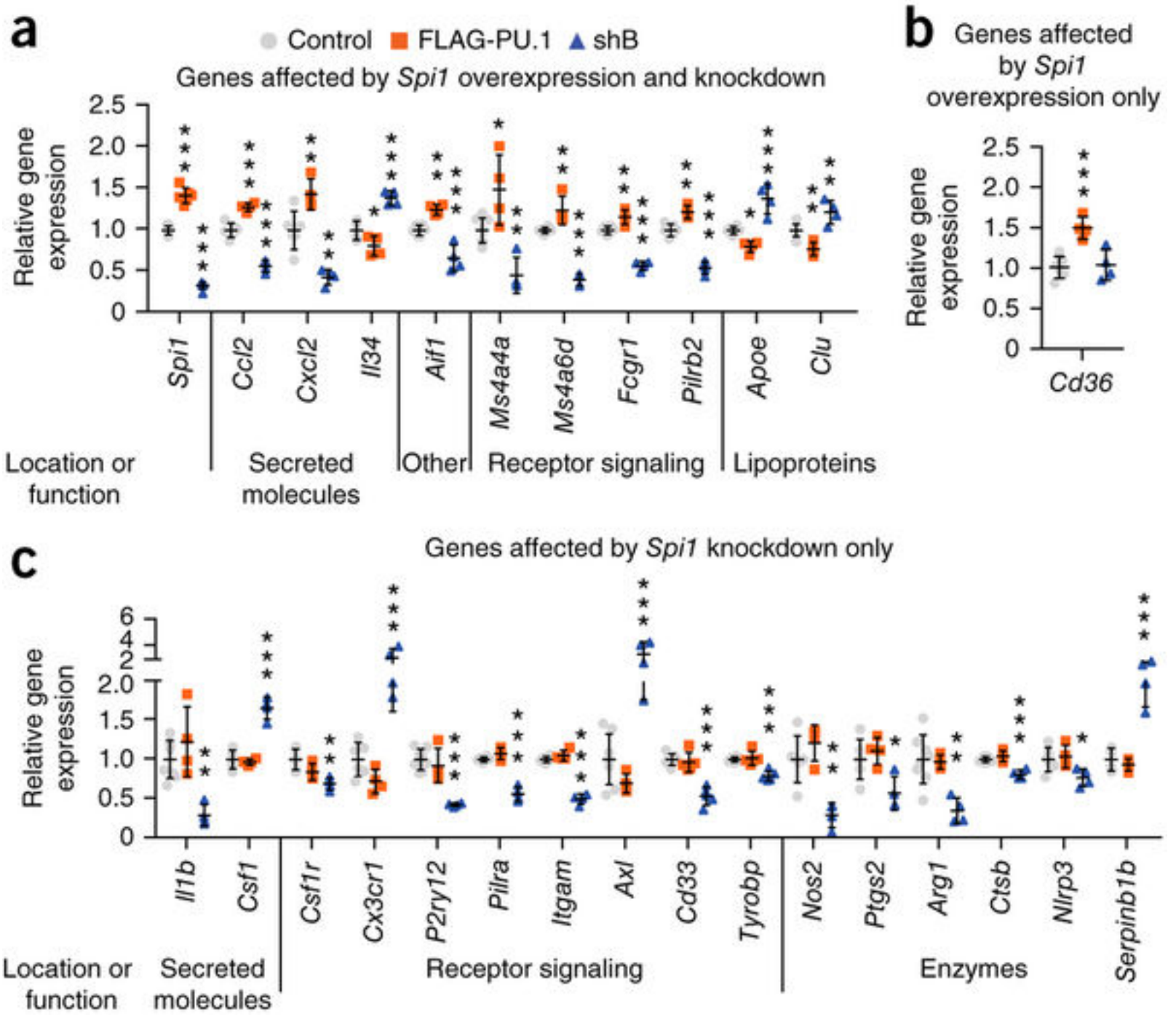

qPCR analysis in transiently transfected and sorted GFP$^+$ BV2 cells with overexpression (FLAG-PU.1) and knockdown (shB) of *Spi1*. Changes in expression levels are grouped for genes with altered levels after (**a**) overexpression and knockdown of *Spi1* and genes with variable expression in BV2 cells with either (**b**) overexpression or (**c**) knockdown of *Spi1*. Values are presented as mean ± s.d.; $n = 4$ samples collected independently. *$P < 0.05$, **$P < 0.01$, ***$P < 0.001$; one-way ANOVA with Dunnett's *post hoc* multiple comparisons test between experimental and control groups. A detailed statistical analysis is reported in Supplementary Table 13.

To further explore the functional impact of variation in *SPI1* expression, we performed qPCR to test whether differential *Spi1* expression in BV2 cells can modulate expression of genes thought to play important roles in AD pathogenesis and/or microglial cell function (Fig. 4, Supplementary Fig. 9 and Supplementary Tables 13 and 14). We found that levels of some of these genes were affected in opposing directions by overexpression and knockdown of *Spi1* (Fig. 4a), while other genes were affected only by overexpression (Fig. 4b) or knockdown (Fig. 4c) or were not affected at all (Supplementary Fig. 9). After knockdown of *Spi1* in BV2 cells, expression of *Cd33*, *Tyrobp*, *Ms4a4a* and *Ms4a6d* (the mouse ortholog of *MS4A6A*) decreased and expression of *Apoe* and *Clu* (also called *ApoJ*) increased (Fig. 4a,c). These data demonstrate that multiple microglial genes, some already implicated in AD, were selectively perturbed by altered expression of *Spi1*.

Discussion

By performing a large-scale genome-wide survival analysis, we discovered multiple loci associated with AAOS (Table 1). The four genome-wide significantly associated loci, *BIN1* ($P = 3.9 \times 10^{-10}$), *MS4A* ($P = 2.3 \times 10^{-9}$), *PICALM* ($P = 9.1 \times 10^{-12}$) and *APOE* ($P = 7.8 \times 10^{-52}$), have been previously reported to be associated with AD risk[1]. Notably, to our knowledge this is the first study showing that the *MS4A* locus is associated with AAOS. The most significantly AAOS-associated SNP at this locus, rs7930318, shows a protective effect (HR = 0.93, CI = 0.90–0.95) in the survival analysis, consistent with the previous IGAP GWAS logistic regression analysis for AD risk (OR = 0.90, CI = 0.87–0.93).

By combining AAOS and CSF-biomarker GWAS results, we provide evidence of AD association at additional loci (Table 2). In particular, rs7867518 at the *VLDLR* locus shows suggestive associations with both AAOS ($P = 9.1 \times 10^{-6}$) and CSF tau ($P = 3.03 \times 10^{-3}$). An adjacent

SNP (rs2034764) in the neighboring gene, *KCNV2*, has been previously reported as having a suggestive association with AAO[7]. VLDLR is a receptor for lipoproteins containing proteins encoded by *APOE*[37] and by *CLU*[38], another AD risk gene. Additionally, the *VLDLR*-5-repeat allele was found to be associated with dementia[37]. This genetic and biochemical evidence suggests *VLDLR* may be linked to AD.

Cis-eQTL analyses of AAOS-associated SNPs revealed limited associations when using data from brain tissue homogenates, yet identified multiple candidate genes when using data from myeloid cells, the top candidate causal cell types for AD based on the stratified LD score regression analysis of AD heritability presented here. This calls attention to the need for careful selection of relevant cell types in eQTL studies of disease associations. In particular, by conducting *cis*-eQTL analyses using monocyte and macrophage datasets, we discovered associations of AAOS-associated SNPs with the expression of *SELL*, *SPI1*, *MYBPC3*, *NUP160*, *MS4A4A*, *MS4A6A* and *SUN2* (Table 3). Furthermore, we replicated the *cis*-eQTL associations of rs1057233 with *SPI1* and *MYBPC3*, rs7930318 with *MS4A4A* and *MS4A6A,* and rs2272918 with *SELL* in an independent monocyte dataset. We further showed that *SPI1* myeloid *cis*-eQTLs and AAOS-associated SNPs are not likely to be colocalized by chance and thus may be in the causal path to AD (Fig. 1). Notably, the minor allele of rs1057233 (G) is suggestively associated with lower AD risk ($P = 5.4 \times 10^{-6}$ and $P = 5.9 \times 10^{-7}$ in IGAP stage I and in IGAP stages I and II combined, respectively)[1] and later AAO ($P = 8.4 \times 10^{-6}$) and is significantly associated with higher CSF $A\beta_{42}$ ($P = 8.24 \times 10^{-4}$), which likely reflects decreased Aβ aggregation and β-amyloid deposition in the brain. Furthermore, it is strongly associated with lower *SPI1* expression in human monocytes ($P = 1.50 \times 10^{-105}$) and macrophages ($P = 6.41 \times 10^{-87}$; Table 3).

Colocalization analyses using coloc[31] and SMR–HEIDI[22] support the hypothesis that the same causal SNP(s) influence *SPI1* expression and AD risk. However, neither conditional nor SMR–HEIDI analyses were able to pinpoint an individual SNP; both approaches identified an LD block tagged by rs1057233, in which one or more SNPs may individually or in combination influence both *SPI1* expression and AD risk. Rs1057233 changes the target sequence and binding of miR-569[32], and its tagging SNPs alter binding motifs of transcription factors including PU.1 itself (Supplementary Table 3 and Supplementary Fig. 7d). Rs1377416 is located in a predicted enhancer in the vicinity of *SPI1* and altered enhancer activity when assayed *in vitro* using a reporter construct transfected in BV2 cells[19]. However, rs1057233 remained significantly associated with AD after conditioning for either rs1377416 ($P = 1.2 \times 10^{-3}$) or the previously reported IGAP GWAS top SNP, rs10838725 ($P = 3.2 \times 10^{-4}$) in the ADGC dataset. Further, the *cis*-eQTL association between rs1057233 and *SPI1* expression remained significant after conditioning for either of these SNPs, whereas conditioning for rs1057233 abolished its *cis*-eQTL associations with *SPI1* (Supplementary Table 9). Thus, rs1057233 and its tagging SNPs likely represent the underlying disease locus and may modulate AD risk through variation in *SPI1* expression. Notably, rs1057233 was previously found to be associated with systemic lupus erythematosus[32], body mass index[39] and proinsulin levels[40] and may contribute to the connection between AD, immune cell dysfunction, obesity and diabetes.

PU.1 binds to *cis*-regulatory elements of several AD-associated genes expressed in human myeloid cells, including *ABCA7*, *CD33*, *MS4A4A*, *MS4A6A*, *TREM2* and *TYROBP* (Fig. 1e and Supplementary Fig. 7). Further, PU.1 binds to active enhancers of *Trem2* and *Tyrobp* in ChIP-seq experiments using mouse BV2 cells[41] or bone marrow-derived mouse macrophages[42]. PU.1 is required for the development and function of myeloid and B-lymphoid cells[43, 44]. In particular, PU.1 expression is dynamically and tightly controlled during haematopoiesis to direct the specification of $CD34^+$ hematopoietic stem and progenitor cells toward the myeloid and B-lymphoid lineage by progressively partitioning into $CD14^+$ monocytes and macrophages, $CD15^+$ neutrophils and $CD19^+$ B cells[45], the cell types highlighted by our stratified LD score regression analysis. Given its selective expression in microglia in the brain (Fig. 2b), PU.1 may modify microglial cell function through transcriptional regulation of target genes that act as downstream modulators of AD susceptibility, as evidenced by the significant enrichment of AD heritability partitioned on the PU.1 cistrome in human myeloid cells (monocytes, $P = 6.94 \times 10^{-3}$; macrophages, $P = 1.65 \times 10^{-3}$; Supplementary Table 12).

In support of this hypothesis, we also demonstrate that changes in PU.1 expression levels alter phagocytic activity in BV2 mouse microglial cells (Fig. 3 and Supplementary Fig. 8). Knockdown of PU.1 expression reduced engulfment of zymosan, whereas overexpression of PU.1 increased engulfment of zymosan, a Toll-like receptor 2 (TLR2) agonist that mimics fungal pathogens. This is in line with previous data showing decreased uptake of $A\beta_{42}$ (also a TLR2 agonist) in primary microglial cells isolated from adult human brain tissue and transfected with siRNA targeting *SPI1*[46]. Notably, several AD-associated genes (for example, *CD33*, *TYROBP*, *TREM2*, *TREML2*, *CR1*, *ABCA7*, *APOE* and *CLU*) have been shown to be involved in the phagocytic clearance of pathogens or host-derived cellular material (for example, β-amyloid, apoptotic cells, myelin debris, lipoproteins, etc.), suggesting a strong link between perturbation of microglial phagocytosis and AD pathogenesis. In addition to *Cd33*, *Tyrobp*, *Apoe* and *Clu*, several genes with roles in phagocytosis are dysregulated by altering *Spi1*

expression, i.e., *Cd36*, *Fcgr1*, *P2ry12*, *Itgam*, *Cx3cr1*, *Axl* and *Ctsb* (Fig. 4a–c), suggesting a collective and coordinated effect of *Spi1* on the phagocytic activity of BV2 cells.

Our genetic analyses show that the protective allele at the *MS4A* locus is associated with lower expression of *MS4A4A* and *MS4A6A* in human myeloid cells, and the BV2 experiment demonstrated that lower expression of *Spi1* (which is protective in humans) led to lower expression of *Ms4a4a* and *Ms4a6d* (the mouse ortholog of *MS4A6A*), which are also associated with reduced AD risk in humans. Transcriptomic and proteomic analyses of microglial cells suggested a microglial homeostatic signature that is perturbed during aging and under pathological conditions[47]. It will be valuable to test whether genetically altered *SPI1* levels prime microglia to exacerbate or alleviate transcriptional responses that occur during aging or disease development. Together with genetic variation in myeloid genes associated with AD as an amplifier, *SPI1* may be a master regulator capable of tipping the balance toward a neuroprotective or neurotoxic microglial phenotype.

PU.1 expression levels regulate multiple myeloid and microglial cell functions[46], including proliferation, survival and differentiation, that could also modulate AD risk. Indeed, expression of *Il34* and *Csf1*, which encode soluble factors that bind to Csf1r and are required for microglial development and maintenance *in vivo*[48], were elevated after knockdown of *Spi1*, while expression of *Csf1r* was reduced (Fig. 4a,c). Notably, inhibition of *Csf1r* in a 3xTg-AD mouse model led to a reduction in the number of microglia associated with β-amyloid plaques and improved cognition[49]. These findings suggest the importance of analyzing cell proliferation, survival, differentiation and migration phenotypes with differential *Spi1* expression, because *Spi1* levels modulate expression of *Ccl2* and *Cxcl2* (Fig. 4a), encoding MCP1 and MIP2α proteins, which help recruit circulating monocytes and neutrophils to the brain to promote neuroinflammation. In addition, knocking down *Spi1* reduced expression of a microgliosis marker *Aif1* (Iba1) along with *Il1b*, *Nos2*, *Ptgs2*, *Arg1* and *Nlrp3* (Fig. 4a,c), suggesting that decreased *Spi1* expression may blunt the proinflammatory response of microglial cells to improve disease outcomes. Notably, expression of *Cx3cr1* and *Axl* were elevated upon knockdown of *Spi1* (Fig. 4c), raising the possibility that beneficial effects of changes in *Spi1* expression are exerted through modulation of synaptic or neuronal clearance. Further experimental investigation of these phenotypes may shed light on the mechanisms of *SPI1* modulation of AD risk. Of note, overexpression and knockdown of *Spi1* in BV2 cells produce different and often opposite changes in expression of the genes profiled here, possibly driving alternative phenotypes that may underlie detrimental and protective roles of PU.1.

In summary, by combining AD survival and endophenotype GWAS analyses, we replicated and discovered multiple genetic loci associated with AAOS. Specifically, we nominate *SPI1* as the gene responsible for disease association at the previously reported *CELF1* locus. *SPI1* encodes PU.1, a transcription factor expressed in microglia and other myeloid cells that directly regulates other AD-associated genes expressed in these cell types. Our data suggest that lower *SPI1* expression reduces risk for AD, suggesting a therapeutic approach to the treatment of AD. Furthermore, we demonstrate that AAOS-associated SNPs within the *MS4A* gene cluster are associated with *cis*-eQTLs in myeloid cells for both *MS4A4A* and *MS4A6A.* Specifically, the allele associated with reduced AD risk is associated with lower *MS4A4A* and *MS4A6A* expression. This is consistent with the observation that lowering *SPI1* expression, which is protective for AD risk, also lowers *MS4A4A* and *MS4A6A* expression. These results reinforce the emerging genetic and epigenetic association between AD and a network of microglial expressed genes[2, 5, 17, 18, 19, 20, 21], highlighting the need to dissect their functional mechanisms.

Methods

Genome-wide survival association study datasets.

The final meta-analysis dataset consists of samples from the Alzheimer's Disease Genetics Consortium (ADGC), Genetic and Environmental Risk in Alzheimer's Disease (GERAD), European Alzheimer's Disease Initiative (EADI), and Cohorts for Heart and Aging Research in Genomic Epidemiology (CHARGE). The study cohorts consist of case–control and longitudinal cohorts. For all studies, written informed consent was obtained from study participants or, for those with substantial cognitive impairment, from a caregiver, legal guardian or other proxy, and the study protocols for all populations were reviewed and approved by the appropriate Institutional review boards. Details of ascertainment and diagnostic procedures for each dataset extend from details previously described[1, 2, 3, 4, 5] and are documented below:

Alzheimer's Disease Genetics Consortium.

The imputed ADGC sample that passed quality control procedures comprised 8,617 AD cases and 9,765 control subjects from GWAS datasets assembled by ADGC. Details of ascertainment and diagnostic procedures for each dataset were as previously described[2].

Genetic and Environmental Risk in Alzheimer's Disease.

Data used in the preparation of this article were obtained from the Genetic and Environmental Risk for Alzheimer's disease (GERAD) Consortium. The imputed GERAD sample comprised 3,177 AD cases and 7,277 controls with available age and gender data. A subset of this sample has been used in this study, comprising 2,615 cases and 1,148 elderly screened controls. Cases and elderly screened controls were recruited by the Medical Research Council (MRC) Genetic Resource for AD (Cardiff University; Institute of Psychiatry, London; Cambridge University; and Trinity College Dublin), the Alzheimer's Research UK (ARUK) Collaboration (University of Nottingham; University of Manchester; University of Southampton; University of Bristol; Queen's University Belfast; and the Oxford Project to Investigate Memory and Aging (OPTIMA), Oxford University); Washington University, St Louis, United States; MRC PRION Unit, University College London; London and the South East Region AD project (LASER-AD), University College London; Competence Network of Dementia (CND) and Department of Psychiatry, University of Bonn, Germany; and the National Institute of Mental Health (NIMH)AD Genetics Initiative. The study drew 6,129 population controls from large existing cohorts with available GWAS data, including the 1958 British Birth Cohort 1958BC; https://www.ebi.ac.uk/ega/studies/EGAS00001000646, the KORA F4 study and the Heinz Nixdorf Recall study. All AD cases met criteria for either probable (NINCDS-ADRDA, DSM-IV) or definite (CERAD) AD. All elderly controls were screened for dementia using the MMSE or ADAS-cog and were determined to be free from dementia at neuropathological examination or had a Braak score of 2.5 or lower. Genotypes from all cases and 4,617 controls were previously included in the AD GWAS by Harold *et al*[3]. Genotypes for the remaining 2,660 population controls were obtained from WTCCC2. Imputation of the dataset was performed using IMPUTE2 and the 1,000 Genomes (http://www.1000genomes.org/) December 2010 reference panel (NCBI build 37.1). The imputed data was then analyzed using logistic regression, including covariates for country of origin, gender, age and three principal components obtained with EIGENSTRAT software based on individual genotypes for the GERAD study participants.

European Alzheimer's Disease Initiative (EADI).

All AD cases were ascertained by neurologists from Bordeaux, Dijon, Lille, Montpelier, Paris, and Rouen, France, with clinical diagnosis of probable AD established according to the DSM-III-R and National Institute of Neurological and Communication Disorders and Stroke-Alzheimer's Disease and Related Disorders Association (NINCDS-ADRDA) criteria[50, 51]. Controls were recruited from Lille, Rouen, Nantes and from the 3C Study[50]. This cohort is a population-based prospective study of the relationship between vascular factors and dementia. It has been carried out in three French cities: Bordeaux (southwest France), Montpelier (southeast France) and Dijon (central eastern France). A sample of noninstitutionalized subjects over 65 years of age was randomly selected from the electoral rolls of each city. Between January 1999 and March 2001, 9,686 subjects meeting the inclusion criteria agreed to participate. Following recruitment, 392 subjects withdrew from the study. Thus, 9,294 subjects were finally included in the study (2,104 in Bordeaux, 4,931 in Dijon and 2,259 in Montpellier). In eight years of follow up, 664 individuals suffered from AD, with 167 prevalent and 497 incident cases. The other individuals were considered as controls. Subjects contributed 9,863 DNA samples that passed DNA quality control, which were genotyped with Illumina Human 610-Quad BeadChips. Following quality control procedures, a final sample of 5,803 3C individuals (387 AD cases and 5,416 controls, cohort dataset) and 2,298 non-3C individuals (1,420 AD cases and 878 controls, case–control dataset) was included in this study.

Cohorts for Heart and Aging Research in Genomic Epidemiology (CHARGE).

The Cardiovascular Health Study (CHS) is a prospective population-based cohort study of risk factors for vascular and metabolic disease that in 1989–1990 enrolled adults aged ≥65 years at four field centers located in North Carolina, California, Maryland and Pennsylvania. The original, predominantly Caucasian, cohort of 5,201 persons was recruited from a random sample of people on Medicare eligibility lists, and an additional 687 African Americans were enrolled subsequently for a total sample size of 5,882. DNA was extracted from blood samples drawn on all persons who consented to genetic testing at their baseline examination in 1989–1990. In 2007–2008, genotyping was performed at the General Clinical Research Center's Phenotyping/Genotyping Laboratory at Cedars-Sinai using the Illumina 370CNV Duo BeadChip system on 3,980 CHS participants who were free of cardiovascular disease (CVD) at baseline. The 1,908 persons excluded for prevalent CVD had prevalent coronary heart disease (*n* = 1,195), congestive heart failure (*n* = 86), peripheral vascular disease (*n* = 93), valvular heart disease (*n* = 20), stroke (*n* = 166) or transient ischemic attack (*n* = 56). Some persons had more than one reason to be excluded and for these individuals only the initial exclusionary event is listed. Because the other cohorts were predominantly white, the African American CHS participants were excluded from this analysis to limit errors secondary to population stratification. Among white participants, genotyping was attempted in 3,397 participants and was successful in 3,295 persons. After excluding persons who had died before the start of the CHS cognition study in 1992, persons who could not be evaluated completely for baseline cognitive status and persons who had dementia other than AD, a sample of 2,049 persons was available. The CHS study protocols were approved by the institutional review boards at the individual participating centers.

The AD sample for this study included all prevalent cases identified in 1992 and incident events identified between 1992 and December 2006. Briefly, persons were examined annually from enrollment to 1999. The examination included a 30-min screening cognitive battery. In 1992–1994 and again in 1997–1999, participants were invited to undergo brain MRI and detailed cognitive and neurological assessment as part of the CHS Cognition Study. Persons with prevalent dementia were identified, and all others were followed until 1999 for the development of incident dementia and AD. Since then, CHS participants at the Maryland and Pennsylvania centers have remained under ongoing dementia surveillance[52].

Beginning in 1988–1989, all participants completed the Modified Mini-Mental State Examination (3MSE) and the DSST at their annual visits, as well as the Benton Visual Retention Test (BVRT), from 1994 to 1998. The Telephone Interview for Cognitive Status (TICS) was used when participants did not come to the clinic. Further information on cognition was obtained from proxies using the Informant Questionnaire for Cognitive Decline in the Elderly (IQCODE) and the dementia questionnaire (DQ). Symptoms of depression were measured with the modified version of the Center for Epidemiology Studies Depression Scale (CES-D). In 1991–1994, 3,608 participants had an MRI of the brain, and this was repeated in 1997–1998. CHS staff also obtained information from participants and next-of-kin regarding vision and hearing, the circumstances of the illness, history of dementia, functional status, pharmaceutical drug use and alcohol consumption. Data on instrumental activities of daily living (IADL) and activities of daily living (ADL) were also collected.

Persons suspected to have cognitive impairment based on the screening tests listed above underwent a neuropsychological and a neurological evaluation. The neuropsychological battery included the following tests: the American version of the National Reading test (AMNART), Raven's Colored Progressive Matrices, California Verbal Learning Test (CVLT), a modified Rey-Osterreith figure, the Boston Naming test, the verbal fluency test, the Block design test, the Trails A and B tests, the Baddeley & Papagno Divided Attention Task, the Stroop test, and the digit span and grooved pegboard tests. The results of the neuropsychological battery were classified as normal or abnormal (defined as > 1.5 s.d. below individuals of comparable age and education) based on normative data collected from a sample of 250 unimpaired subjects. The neurological exam included a brief mental status examination, as well as a complete examination of other systems. The examiner also completed the Unified Parkinson's Disease Rating Scale (UPDRS) and the Hachinski Ischemic Scale. After completing the neurological exam, the neurologist classified the participant as normal, having mild cognitive impairment (MCI) or having dementia.

International diagnostic guidelines, including the NINCDS-ADRDA criteria for probable and possible AD and the ADDTC's State of California criteria for probable and possible vascular dementia (VaD) with or without AD were followed. CHS identified three subtypes: possible/probable AD without VaD (categorized as pure AD, included in all-AD); mixed AD (for cases that met criteria for both AD and VaD, included in all-AD); and possible/probable VaD without AD (excluded from the current study).

The Framingham Heart Study (FHS) is a three-generation, single-site, community-based, ongoing cohort study initiated in 1948. It now comprises three generations of participants including the Original cohort followed since 1948 (n = 5,209)[53], their Offspring and spouses of the offspring (n = 5,216) followed since 1971[54]; and children from the largest Offspring families enrolled in 2000 (Gen 3)[55]. Participants in the Original and Offspring cohorts are used in these analyses, but Gen 3 participants were not included since they are young (mean age 40 ± 9 years in 2000) and none had developed AD. The Original cohort enrolled 5,209 men and women who comprised two-thirds of the adult population then residing in Framingham, Massachusetts. Survivors continue to receive biennial examinations. The Offspring cohort comprises 5,124 persons (including 3,514 biological offspring) who have been examined approximately once every 4 years. Almost all the FHS Original and Offspring participants are white/Caucasian. FHS participants provided DNA samples and consent for genotyping in the 1990s. All available eligible participants were genotyped at Affymetrix (Santa Clara, CA) through an NHLBI-funded SNP-Health Association Resource (SHARe) project using the Affymetrix GeneChip Human Mapping 500K Array Set and 50K Human Gene Focused Panel. In 272 persons, small amounts of DNA were extracted from stored whole blood and required whole-genome amplification before genotyping. Cell lines were available for most of the remaining participants. Genotyping was attempted in 5,293 Original and Offspring cohort participants, and of these, 4,425 persons met QC criteria. Failures (call rate <97%, extreme heterozygosity or high Mendelian error rate) were largely restricted to persons with whole-genome amplified DNA and DNA extracted from stored serum samples. In addition, since the persons with whole-genome amplified DNA represent a group of survivors who may differ from the others, we included whole-genome amplified status as a covariate in FHS analyses. After exclusion of prevalent dementia, dementia other than AD and missing values, a sample of 2,208 participants was available for this project. The FHS component of this study was approved by the Institutional Review Board of the Boston Medical Center.

The Original cohort of the FHS has been evaluated biennially since 1948, was screened for prevalent dementia and AD in 1974–1976 and has been under surveillance for incident dementia and AD since then[56, 57, 58]. The Offspring have been examined once every 4 years and have been screened for prevalent dementia with a neuropsychological battery and brain MRI[59, 60]. To be consistent with the sampling frame for the AGES and CHS samples, we excluded FHS subjects with a baseline age < 65 yrs at the time of DNA draw, which was in the 1990s. To minimize survival biases, Original cohort and Offspring participants who developed dementia before the date of DNA draw were treated as prevalent cases, and subsequent events in the Original cohort occurring before December 2006 were included in the incident analyses.

At each clinic exam, participants receive questionnaires, physical examinations and laboratory testing; between examinations they remain under surveillance (regardless of whether or not they live in the vicinity) via physician referrals, record linkage and annual telephone health history updates. Methods used for dementia screening and follow-up have been previously described[56, 61]. Briefly, surviving cohort members who attended biennial examination cycles 14 and 15 (May 1975 to November 1979) were administered a standardized neuropsychological test battery to establish a dementia-free cohort. Beginning at examination cycle 17 (1982), the MMSE was administered biennially to the cohort. A MMSE score below the education-specific cutoff score, a decline of 3 or more points on subsequent administrations, a decline of more than 5 points compared with any previous examination or a physician or family referral prompted further in-depth testing. The Offspring cohort that was enrolled in 1971 has undergone eight re-examinations, one approximately every 4 years. Starting at the second Offspring examination, participants were questioned regarding any subjective memory complaints, and since the fifth Offspring examination, participants have been administered the MMSE at each visit. In addition, concurrent with the seventh and eighth Offspring examinations (between 1999 and 2004 and between 2005 and 2009, respectively), surviving Original cohort and all eligible and consenting Offspring participants have undergone volumetric brain MRI and neuropsychological testing[59, 60]. The neuropsychological test battery included the Reading subtest of the Wide Range Achievement Test (WRAT-3), the Logical Memory and the Paired Associates Learning tests from the Wechsler Memory Scale, the Visual Reproduction and Hooper Visual Organization Tests, Trails A and B, the Similarities subtest from the Wechsler Adult Intelligence test, the 30-item version of the Boston Naming Test and, at the second assessment only, the digit span, controlled word association and clock drawing tests. Offspring participants suspected to have cognitive impairment based on their MMSE scores, participant, family or physician referral, hospital records or performance in the neuropsychological test battery described above were referred for more detailed neuropsychological and neurological evaluation.

Each participant thus identified underwent baseline neurologic and neuropsychological examinations. Neurologists trained in geriatric behavioral assessment supplemented their clinical assessment with a few structured cognitive tests and administered the Clinical Dementia Rating (CDR). Persons were reassessed systematically for the onset of at least mild dementia. A panel consisting of at least one neurologist (S. Auerbach, P.A. Wolf (Department of Neurology, Boston University School of Medicine) or S.S.) and one neuropsychologist (R. Au, Department of Anatomy and Neurobiology, Boston University School of Medicine) reviewed all available medical records to arrive at a final determination regarding the presence or absence of dementia, the date of onset of dementia and the type of dementia. For this determination, we used data from the neurologist's examination, neuropsychological test performance, Framingham Study records, hospital records, information from primary care physicians, structured family interviews, computed tomography records and MRI records, as well as autopsy confirmation when available. All individuals identified as having dementia satisfied the DSM-IV criteria, had dementia severity equivalent to a CDR of 1 or greater and had had symptoms of dementia for at least 6 months. All individuals identified as having Alzheimer's-related dementia met the NINCDS-ADRDA criteria for definite, probable or possible AD. Vascular dementia was diagnosed using the ADDTC criteria but the presence of vascular dementia did not disqualify a participant from obtaining a concomitant diagnosis of AD if indicated. The recruitment of Original cohort participants at FHS occurred long before DNA collection, with the result that either the majority of dementia events in the FHS (although ascertained prospectively) were prevalent at the time of DNA collection or persons with dementia died before DNA draw and were thus excluded from analyses of incident disease. Due to the limited number of incident dementia and AD events in the Framingham Offspring, only the Original cohort were included in our analyses of incident events.

The Rotterdam Study enrolled inhabitants from a district of Rotterdam, the Netherlands (Ommoord), aged ≥ 55 years (*N* = 7,983, virtually all white) at the baseline examination in 1990–1993 when blood was drawn for genotyping[62]. It aims to examine the determinants of disease and health in the elderly with a focus on neurogeriatric, cardiovascular, bone and eye disease. All inhabitants of Ommoord aged ≥55 years (*n* = 10,275) were invited, and the participation rate was 78%. All participants gave written informed consent to retrieve information from treating physicians. Baseline measurements were obtained from 1990 to 1993 and consisted of an interview at home and two visits to the research center for physical examination. Survivors have been re-examined three times: in 1993–1995, 1997–1999 and 2002–2004. All persons attending the baseline examination in 1990–1993 consented to genotyping and had DNA extracted. This DNA was genotyped using

the Illumina Infinium II HumanHap550chip v3.0 array in 2007–2008 according to the manufacturer's protocols. Genotyping was attempted in persons with high-quality extracted DNA (*n* = 6,449). From these 6,449, samples with low call rate (<97.5%, *n* = 209), with excess autosomal heterozygosity (heterozygosity > 0.336, *n* = 21), with sex mismatch (*n* = 36) or with outliers identified by the IBS clustering analysis (>3 s.d. from population mean, *n* = 102; or IBS probabilities >97%, *n* = 129) were excluded from the study population, with some persons meeting more than one exclusion criterion. After exclusions, 5,974 samples were available with good quality genotyping data; 42 persons were excluded since they did not undergo cognitive screening at baseline and hence their cognitive statuses were uncertain. An additional 61 persons were excluded because they suffered from dementia other than AD at baseline. After exclusion of prevalent dementia, a sample of 5,752 persons was available. The Rotterdam study (including its brain MRI and neurological components) was approved by the institutional review board (Medical Ethics Committee) of the Erasmus Medical Center and the Netherlands Ministry of Health, Welfare and Sports Participants were screened for prevalent dementia in 1990–1993 using a three-stage process; those free of dementia remained under surveillance for incident dementia, a determination made using records linkage and assessment at three subsequent re-examinations. We included all prevalent cases and all incident events up to 31 December 2007.

Screening was done with the MMSE and geriatric mental schedule (GMS) organic level for all persons. Screen-positives (MMSE < 26 or GMS organic level > 0) underwent the CAMDEX. Persons who were suspected of having dementia underwent more extensive neuropsychological testing. When available, imaging data were used. In addition, all participants have been continuously monitored for major events (including dementia) through automated linkage of the study database with digitized medical records from general practitioners, the Regional Institute for Outpatient Mental Health Care and the municipality. In addition, physician files from nursing homes and general practitioner records of participants who moved out of the Ommoord district were reviewed twice a year. For suspected dementia events, additional information (including neuroimaging) was obtained from hospital records and research physicians discussed available information with a neurologist experienced in dementia diagnosis and research to verify all diagnoses. Dementia was diagnosed in accordance with internationally accepted criteria for dementia (DSM-III-R) and AD using the NINCDS-ADRDA criteria for possible, probable and definite AD. The National Institute of Neurological Disorders and Stroke-Association Internationale pour la Recherche et l'Enseignement en Neurosciences (NINDS-AIREN) criteria were used to diagnose vascular dementia. The final diagnosis was determined by a panel composed of a neurologist, a neurophysiologist and a research physician, and the diagnoses of AD and VaD were not mutually exclusive.

Power calculation.

To determine the power to detect genetic variants associated with age at onset, we ran analyses using Proc Power in SAS. The analysis was run using minor allele frequencies ranging from 0.05 to 0.50, OR 1.1 to 1.75 and a sample size of 45,000. Other factors, such as genetic heterogeneity and gene–environment interactions, are likely to affect these estimates. Alpha was adjusted to 5×10^{-8}. For variants with a MAF of 0.15, we would have approximately 80% power to detect effects for OR > 1.23 or OR < 0.81; for variants with a MAF of 0.3, we would have approximately 80% power to detect effects for OR > 1.18 (or OR < 0.85).

CSF biomarker datasets.

CSF samples were obtained from Knight-ADRC (*N* = 805), ADNI-1 (*N* = 390), ADNI-2 (*N* = 397), Biomarkers for Older Controls at Risk for Dementia (BIOCARD; *N* = 184), Mayo Clinic (*N* = 433), Lund University (Swedish; *N* = 293), University of Pennsylvania (Penn; *N* = 164), University of Washington (*N* = 375), Parkinson's Progression Markers Initiative (*N* = 500) and Saarland University (German; *N* = 105) studies.

Cases were diagnosed with dementia of the Alzheimer's type (DAT) according to the NINCDS-ADRDA[20]. Control individuals were evaluated using the same criteria and showed no symptoms of cognitive impairment. Written informed consent was obtained for all participants and prior Institutional Review Board approval was obtained at each participating institution. We obtained 787 additional samples with biomarker data used in the analyses from the ADNI database (http://adni.loni.usc.edu/). ADNI was launched in 2003 as a public–private partnership, led by M.W. Weiner. The primary goal of ADNI has been to test whether serial MRI, positron emission tomography (PET), other biological markers and clinical and neuropsychological assessment can be combined to measure the progression of mild cognitive impairment (MCI) and early AD.

CSF in all studies was collected in a standardized manner[12, 63, 64, 65, 66]. Biomarker measurements within each study were conducted using internal standards and controls to achieve consistency and reliability. However, differences in the measured values between studies were observed, which are likely due to differences in the antibodies and technologies used for quantification (standard ELISA with Innotest

for Knight-ADRC, UW, Swedish, German and Mayo, versus Luminex with AlzBio3 for ADNI-1, ADNI-2, BIOCARD and Penn), ascertainment and/or handling of the CSF after collection. CSF $A\beta_{42}$ and $ptau_{181}$ values were log-transformed in order to approximate a normal distribution. Because the CSF biomarker values were measured using two different platforms (standard ELISA with Innotest and Luminex with AlzBio3), we did not combine the raw data. For the combined analyses, we standardized the mean of the log-transformed values from each dataset to zero. No differences in the transformed and standardized CSF values were found between cohorts. We also performed meta-analyses for the most significant SNPs by combining the *P* values for each independent dataset using METAL[67]. No major differences were found between the joint analyses and the meta-analyses.

Quality control.

For survival analysis, we excluded cases with AAO < 60 and cases with prevalent stroke. For CSF analysis, individuals under age 45 years were removed because prior studies have demonstrated that the relationship between CSF $A\beta_{42}$ levels and age appears to differ in individuals below 45 years versus those above 45 years[68]. Of the remaining individuals in both analyses, we excluded individuals who had > 5% missing genotype rates, who showed a discrepancy between reported sex and sex estimated on the basis of genetic data or who showed evidence of non-European ancestry based on principal component analysis using PLINK1.9[69]. We identified unanticipated duplicates and cryptic relatedness using pair-wise genome-wide estimates of proportion identity by descent (IBD) using PLINK. When a pair of duplicate samples or a pair of samples with cryptic relatedness was identified, the sample with the lower genotyping call rate was removed. We excluded potentially related individuals so that all remaining individuals had kinship coefficients < 0.05. Finally, we excluded individuals with missing disease status, age or gender information.

To control for genotype quality, we excluded SNPs with missing genotypes in > 5% of individuals in each dataset for survival analysis and > 2% for CSF association analysis. For the EADI cohort, variants with minor allele frequency < 1%, Hardy-Weinberg $P < 1 \times 10^{-6}$ and missingness > 2% were removed before imputation. Genome-wide genotype imputation was performed using IMPUTE2[70] with 1,000 Genomes reference haplotypes. We excluded imputed SNPs with an IMPUTE2 quality score < 0.5 for survival analysis. For CSF association, we excluded SNPs with an IMPUTE2 quality score of < 0.3 since the dataset was only used for follow-up. In the ADGC, GERAD, CHARGE and CSF datasets, we then removed SNPs that failed the Hardy-Weinberg equilibrium in controls calculated based on the imputed best-guess genotypes using a *P* value threshold of 1×10^{-6}. We excluded SNPs with minor allele frequency ≤ 0.02. Finally, we excluded SNPs with available statistics in only one consortium dataset in the meta-analysis. The number of filtered samples and SNPs in each of the above steps are recorded in Supplementary Table 1.

Genome-wide survival association study.

We conducted a genome-wide Cox proportional hazards regression[71] assuming an additive effect from SNP dosage. The Cox proportional hazard regression was implemented in the R survival analysis package. We incorporated sex, site and the first three principal components from EIGENSTRAT[29] in all our regression models to control for their effects. For EADI, sex and four principal components were included in the model. For the Cox model, the time scale is defined as age in years, where 'age' is age at onset for cases and age at last assessment for controls. The formula applied is as followed:

$$h(t|X) = h_0(t)\exp\left(\sum_{i=1}^{p}\beta_i X_i\right)$$

where $X = (X_1, X_2, ..., Xp)$ are the observed values of covariates for subject *i*. The Cox model has previously been shown to be applicable to case–control datasets without an elevated type-1 error rate nor overestimation in effect sizes[72, 73]. The model assumes log-linearity and proportional hazards. The assumption of log-linearity is common in the additive logistic regression used in a typical GWAS. We validated the assumption of proportional hazards assumed by the Cox model by conducting the Schoenfeld test in the 22 prioritized SNPs. None of the SNPs has a Schoenfeld *P* value, which is the *P* value for Pearson product–moment correlation between the scaled Schoenfeld residuals and time, of less than 0.035 (multiple test correction threshold = 0.00227) in any of the seven cohorts. Further, only three of the 148 *P* values were less than 0.05, suggesting that the time-proportionality assumption is unlikely to be violated in these associations (Supplementary Table 1). Similarly, the Schoenfeld test was conducted for all 22 SNP association models on the covariates in the ADGC and GERAD cohort (Supplementary Table 1). We also examined the effect sizes of our candidate SNPs in these cohorts and found consistent effect sizes (Supplementary Fig. 3) in the three retrospective case–control cohorts (ADGC, GERAD and EADI case–control) and four prospective cohorts (EADI-prospective, CHARGE FHS, CHS and Rotterdam).

After the analysis of each dataset, we carried out an inverse-variance meta-analysis on the results using METAL[25], applying a genomic control to adjust for inflation in each dataset. Of the 751 suggestive SNPs ($P < 1 \times 10^{-5}$), we found that these SNPs showed lower standard errors and confidence intervals as the number of cohorts increased, showing consistent directionalities of effect. Particularly, the average standard error for SNPs showing 1–7 consistent directionalities ranges from 0.171, 0.109, 0.0744, 0.0346, 0.0234 and 0.0173 to 0.01795 (Supplementary Fig. 1b). Thus, we limited our final analysis to SNPs that showed consistent directionalities of effect in at least six of the seven datasets included in the meta-analysis. The association graphs of results from loci of interest were plotted using LocusZoom[74].

CSF biomarker association analysis.

For the CSF datasets, we performed multivariate linear regression for CSF $A\beta_{42}$ tau and $ptau_{181}$ association, adjusting for age, gender, site and the first three principal components, using PLINK.

eQTL analysis.

We examined the effect of top survival and CSF SNPs on gene expression using published databases. For general brain expression eQTL analysis, we queried the BRAINEAC eQTL data provided by the UK human Brain Expression Consortium (see URLs).

We conducted leukocyte-specific analysis using the Cardiogenics dataset[26], which is composed of 738 monocytes and 593 macrophages samples. For each probeset-imputed SNP pair, a simple linear regression was used to analyze the data separately for monocytes and macrophages:

$$y_i = \alpha + \beta x_i + \varepsilon_i,\ 1 \le i \le n,\ \varepsilon_i \sim N\left(0, \sigma^2\right)$$

where *i* is the subject index, *x* is the effective allele copy number, and y_i is the covariates-adjusted, inverse-normal transformed gene expression. Significance of *cis* (SNP within ±1 Mb of the closest transcript end) eQTL effects were quantified with a Wald test on the ordinary least-squares (OLS) estimator of the coefficient *β*, obtained with R. The distribution of the Wald test *P* values under the null hypothesis of no correlation between genotype and gene expression was estimated by rerunning the same analysis on a null dataset, obtained by permuting the expression samples identifiers. For additional monocyte eQTL analysis, we queried statistics from Fairfax *et al.*[27] to validate findings in the Cardiogenics dataset.

For conditional analysis, we performed analysis for *SPI1* (probe: ILMN_1696463) against all SNPs within ±2 Mb from the closest transcript end by including the effective allele copy numbers of the following SNPs as covariates in the linear regression model, one at a time: rs1057233, rs10838698, rs7928163, rs10838699, rs10838725 and rs1377416. Significance was again assessed with a two-sided Wald test on the OLS estimator of the coefficient *β*.

Gene-expression analysis in human and mouse brain cell types.

Cell-type-specific gene expression in the human and mouse brain was queried from brain RNA-seq databases described in Zhang *et al.*[28,29] and Bennett *et al.*[30] and plotted using custom R scripts (see URLs). The mouse FAC-sorted astrocytes and immunopanned astrocytes were collapsed into a single astrocyte cell type.

Epigenetic analysis in human myeloid cell types.

We used HaploReg[33] to annotate the regulatory element of the significantly associated SNPs and their tagging SNPs. The myeloid chromatin marks/states and PU.1 ChIP-seq data at genetic loci were further examined through the Washington University Epigenome browser[75] using the public Roadmap Epigenomics Consortium public tracks hub as well as custom track hubs for human monocytes and macrophages (hg19; see URLs).

Colocalization (coloc and SMR/HEIDI) analyses.

Colocalization analysis of genetic variants associated with AD and myeloid gene expression was performed using AAOS GWAS SNP and myeloid (monocyte and macrophage) eQTL datasets from Cardiogenics as inputs. Overlapping SNPs were retained within the hg19 region chr11:47100000–48100000 for the *SPI1* locus, chr11:59500000–60500000 for the *MS4A* locus and chr1:169300000–170300000 for the *SELL* locus. Colocalization analysis of AD-associated and gene-expression-associated SNPs was performed using the coloc.abf function in the 'coloc' R package (v2.3-1). Default settings were used as prior probability of association: 1×10^{-4} for trait 1 (gene expression), 1×10^{-4} for trait 2 (AD) and 1×10^{-5} for both traits. SMR/HEIDI (v0.65) analysis was performed as described in Zhu *et al.*[22] and the companion

website (see URLs). The ADGC subset of the IGAP GWAS dataset was used to perform the LD calculations.

Partitioned heritability analysis using LD score regression.

We used LDSC (LD SCore, v1.0.0) regression analysis[24] to estimate heritability of AD and schizophrenia from GWAS summary statistics (excluding the *APOE* (chr19:45000000–45800000) and *MHC*/*HLA* (chr6:28477797–33448354) regions) partitioned by PU.1 ChIP-seq binding sites in myeloid cells, as described in the companion website (see URLs), and controlling for the 53 functional annotation categories of the full baseline model. GWAS summary statistics for AD and schizophrenia (SCZ) were downloaded from the IGAP consortium[1] (stage 1 dataset) and the Psychiatric Genomics Consortium (PGC[25]; pgc.cross.scz dataset), respectively (see URLs). *SPI1* (PU.1) bindings sites were downloaded as filtered and merged ChIP-seq peaks in BED format from the ReMap database[76] (GEO: GSE31621; *SPI1*, blood monocyte and macrophage datasets[34]). *SPI1* (PU.1) and POLR2AphosphoS5 binding sites were downloaded as broad ChIP-seq peaks in BED format from the Encode portal[36, 77] (DCC: ENCSR037HRJ; GEO: GSE30567; HL60 dataset; see URLs).

Phagocytosis assay.

The BV2 mouse microglial cell line was kindly provided by M. Diamond (UT Southwestern Medical Center). BV2 cells were cultured in DMEM (Gibco 11965), supplemented with 5% FBS (Sigma F4135) and 100 U/mL penicillin–streptomycin (Gibco 15140). Routine testing of cell lines using MycoAlert PLUS mycoplasma detection kit (Lonza) showed that BV2 cells were negative for mycoplasma contamination. pcDNA3-FLAG-PU.1 was a gift from C. Vakoc[78] (Addgene plasmid 66974). pGFP-V-RS with either nontargeting shRNA or PU.1-targeting shRNAs was purchased from OriGene Technologies (TG502008). The pHrodo red zymosan conjugate bioparticles from Thermo Fisher (P35364) were used to assess phagocytic activity. For transient transfections, 200,000 cells were seeded in a 24-well plate. On the next day, cells were washed with PBS (Gibco 14190) and medium was changed to 400 µL DMEM, supplemented with 2% FBS without antibiotics. Transfection mixes of 0.5 µg pcDNA3 or 0.5 µg pcDNA3-FLAG-PU.1 with 0.5 µg pCMV-GFP for overexpression of mouse PU.1 and 1 µg pGFP-V-RS-shSCR, -shA, -shB and -shD for knockdown of mouse PU.1 were prepared with 2 µL of Lipofectamine 2000, incubated for 20 min at room temperature (23 °C) and added to each well. After 8 h of incubation, 1 mL of growth medium was added to each well and plates were incubated for 2 d. Then the medium was replaced with 500 µl of fresh medium, and 25 µg of bioparticles were added to cells for 3 h incubation. Bioparticle uptake was verified with a fluorescent microscope; then the cells were collected with trypsin (Gibco 25200), washed with PBS once and resuspended in 500 µL PBS with 1% BSA. Cells were kept on ice, and phagocytic activity was analyzed on an LSR II flow cytometer (BD Biosciences). At least 30,000 events were collected in each experiment, gated on FSC-A/SSC-A and further on FSC-A/FSC-W dot plots to analyze populations of viable single cells. Data were quantified using FCS Express 5 (De Novo Software) and GraphPad Prism 7 (GraphPad Software). Cells pretreated with 1 µM Cytochalasin D for 30 min before and during the uptake of bioparticles were used as a negative control. The population of $GFP^+pHrodo^+$ cells in each condition was used to quantify the phagocytic index: (percentage of $pHrodo^+$ cells in GFP^+ gated population) × (the geometric mean of pHrodo intensity)/10^6; and represented as phagocytic activity. Three independent experiments were performed with two technical replicates without randomization of sample processing, $n = 3$. The researcher was not blinded to sample identification. Differences between means of data were analyzed with one-way ANOVA and Sidak's *post hoc* multiple-comparisons test between selected groups, with a single pooled variance. Adjusted *P* values for each comparison are reported; nonsignificant differences are not reported.

Western blotting.

BV2 cells transiently transfected as described for the phagocytosis assay were collected with trypsin after 48 h of incubation, washed with PBS and resuspended in PBS with 1% BSA. Cells from the same treatment were pooled and sorted on FACSARIA III (BD Biosciences) into GFP^+ and GFP^- populations, pelleted at 2,000 rpm and lysed in RIPA buffer (50 mM Tris-HCl pH 7.4, 150 mM NaCl, 1% NP-40, 0.5% sodium deoxycholate, 0.1% SDS and Complete protease inhibitor tablets (Roche)) with one freeze–thaw cycle and 1 h incubation on ice. Protein concentration was quantified using the BCA kit (Thermo Fisher #23225). Equal amounts of protein were separated by electrophoresis in Bolt 4 12% Bis-Tris Plus gels with MOPS SDS running buffer and transferred using the iBlot 2 nitrocellulose transfer stack. Membranes were blocked and probed with antibodies against PU.1 (Cell Signaling, #2266) and β-actin (Sigma, #A5441) in 3% nonfat dry milk in TBS / 0.1% Tween-20 buffer. Secondary antibody staining was visualized using WesternBright ECL HRP Substrate Kit (Advansta K-12045) and ChemiDoc XRS+ (BioRad). Images were quantified using ImageJ (NIH) and GraphPad Prism 7 (GraphPad Software). Two independent experiments were performed without randomization of sample processing, $n = 2$. The researcher was not blinded to sample identification. Differences between means of data were analyzed with one-way ANOVA and Sidak's *post hoc* multiple-comparisons test between selected groups, with a single pooled variance. Adjusted *P* values for each comparison are reported.

Quantitative PCR.

Sorted GFP$^+$ BV2 cells after overexpression or knockdown of PU.1 were collected as described for western blotting. Cell pellets were lysed in QIAzol reagent and RNA was isolated with RNAeasy Mini kit according to the manufacturer's instructions (Qiagen) including the Dnase treatment step with RNase-free DNase set (Qiagen). Quantities of RNA were measured using Nanodrop 8000 (Thermo Scientific) and reverse transcription was performed with 1–2 µg of total RNA using High-Capacity RNA-to-cDNA kit (Thermo Fisher Scientific). qPCR was performed on QuantStudio 7 Flex Real-Time PCR System (Thermo Fisher Scientific) using Power SYBR Green Master Mix (Applied Biosystems) with one-step PCR protocol. We used 3 ng of cDNA for all genes except *Ms4a4a*, for which we used 24 ng of cDNA in a 10-µL reaction volume. Primers were from PrimerBank[79] or designed using Primer-BLAST program (NCBI) and are listed in Supplementary Table 14. Ct values were averaged from two technical replicates for each gene. The geometric mean of average Ct for the housekeeping genes *Gapdh*, *B2m* and *Actb* was used as a reference that was subtracted from the average Ct for a gene of interest (dCt). Gene expression levels were log transformed (2^{-dCt}) and related to the combined mean values of pcDNA3 and pGFP-V-RS-shSCR control samples in each sort, giving the relative expression for each gene of interest. Data were visualized in GraphPad Prism 7 (GraphPad Software). Four independent experiments were performed without randomization of sample processing, $n = 4$. The researcher was not blinded to sample identity. Differences between means were analyzed using one-way ANOVA and Dunnett's *post hoc* multiple-comparisons test between experimental and control groups, with a single pooled variance. Adjusted *P* values for each comparison are reported in Supplementary Table 13.

Data availability.

Summary statistics for the genome-wide survival analyses are posted on the NIA Genetics of Alzheimer's Disease Data Storage (NG0058). A Supplementary Methods Checklist is available.

Code availability.

Codes for analyses are available at a public GitHub repository (https://github.com/kuanlinhuang/AD_SPI1_project).

URLs.

BRAINEAC, http://caprica.genetics.kcl.ac.uk/BRAINEAC; LDSC software, http://www.github.com/bulik/ldsc; baseline and cell type group annotations, http://data.broadinstitute.org/alkesgroup/LDSCORE/; stratified LD score regression companion website, https://github.com/bulik/ldsc/wiki/Partitioned-Heritability; SMR/HEIDI software and companion website, http://cnsgenomics.com/software/smr; Brain RNA-seq, http://web.stanford.edu/group/barres_lab/brainseq2/brainseq2.html; WashU EpiGenome Browser, http://epigenomegateway.wustl.edu/browser; custom tracks for human monocytes and macrophages, http://www.ag-rehli.de/TrackHubs/hub_MOMAC.txt; International Genomics of Alzheimer's Project (IGAP), http://web.pasteur-lille.fr/en/recherche/u744/igap/igap_download.php; Psychiatric Genomics Consortium (PGC), https://www.med.unc.edu/pgc/results-and-downloads; ReMap database, http://tagc.univ-mrs.fr/remap; Encode portal https://www.encodeproject.org/; NIAGADS, https://www.niagads.org.

Additional information

Publisher's note: Springer Nature remains neutral with regard to jurisdictional claims in published maps and institutional affiliations.

References

1. Lambert, J.-C. *et al*. Meta-analysis of 74,046 individuals identifies 11 new susceptibility loci for Alzheimer's disease. *Nat. Genet.* **45**, 1452–1458 (2013).
2. Naj, A.C. *et al*. Common variants at *MS4A4*/*MS4A6E*, *CD2AP*, *CD33* and *EPHA1* are associated with late-onset Alzheimer's disease. *Nat. Genet.* **43**, 436–441 (2011).
3. Harold, D. *et al*. Genome-wide association study identifies variants at *CLU* and *PICALM* associated with Alzheimer's disease. *Nat. Genet.* **41**, 1088–1093 (2009).
4. Seshadri, S. *et al*. Genome-wide analysis of genetic loci associated with Alzheimer disease. *J. Am. Med. Assoc.* **303**, 1832–1840 (2010).
5. Hollingworth, P. *et al*. Common variants at *ABCA7*, *MS4A6A*/*MS4A4E*, *EPHA1*, *CD33* and *CD2AP* are associated with Alzheimer's disease. *Nat. Genet.* **43**, 429–435 (2011).

6. Naj, A.C. *et al*. Effects of multiple genetic loci on age at onset in late-onset Alzheimer disease: a genome-wide association study. *JAMA Neurol.* **71**, 1394–1404 (2014).

7. Kamboh, M.I. *et al*. Genome-wide association analysis of age-at-onset in Alzheimer's disease. *Mol. Psychiatry* **17**, 1340–1346 (2012).

8. Bennett, C. *et al*. Evidence that the *APOE* locus influences rate of disease progression in late onset familial Alzheimer's Disease but is not causative. *Am. J. Med. Genet.* **60**, 1–6 (1995).

9. Slooter, A.J. *et al*. Risk estimates of dementia by apolipoprotein E genotypes from a population-based incidence study: the Rotterdam Study. *Arch. Neurol.* **55**, 964–968 (1998).

10. Thambisetty, M., An, Y. & Tanaka, T. Alzheimer's disease risk genes and the age-at-onset phenotype. *Neurobiol. Aging* **34**, 2696 e1–2696.e5 (2013).

11. Jones, E.L. *et al*. Evidence that *PICALM* affects age at onset of Alzheimer's dementia in Down syndrome. *Neurobiol. Aging* **34**, 2441 e1–2441.e5 (2013).

12. Cruchaga, C. *et al*. GWAS of cerebrospinal fluid tau levels identifies risk variants for Alzheimer's disease. *Neuron* **78**, 256–268 (2013).

13. Kauwe, J.S.K. *et al*. Alzheimer's disease risk variants show association with cerebrospinal fluid amyloid beta. *Neurogenetics* **10**, 13–17 (2009).

14. Gusev, A. *et al*. Integrative approaches for large-scale transcriptome-wide association studies. *Nat. Genet.* **48**, 245–252 (2016).

15. Jonsson, T. *et al*. Variant of *TREM2* associated with the risk of Alzheimer's disease. *N. Engl. J. Med.* **368**, 107–116 (2013).

16. Guerreiro, R. *et al*. *TREM2* variants in Alzheimer's disease. *N. Engl. J. Med.* **368**, 117–127 (2013).

17. Bradshaw, E.M. *et al*. *CD33* Alzheimer's disease locus: altered monocyte function and amyloid biology. *Nat. Neurosci.* **16**, 848–850 (2013).

18. Zhang, B. *et al*. Integrated systems approach identifies genetic nodes and networks in late-onset Alzheimer's disease. *Cell* **153**, 707–720 (2013).

19. Gjoneska, E. *et al*. Conserved epigenomic signals in mice and humans reveal immune basis of Alzheimer's disease. *Nature* **518**, 365–369 (2015).

20. Chan, G. *et al*. CD33 modulates *TREM2*: convergence of Alzheimer loci. *Nat. Neurosci.* **18**, 1556–1558 (2015).

21. Raj, T. *et al*. Polarization of the effects of autoimmune and neurodegenerative risk alleles in leukocytes. *Science* **344**, 519–523 (2014).

22. Zhu, Z. *et al*. Integration of summary data from GWAS and eQTL studies predicts complex trait gene targets. *Nat. Genet.* **48**, 481–487 (2016).

23. GTEx Consortium. The Genotype-Tissue Expression (GTEx) project. *Nat. Genet.* **45**, 580–585 (2013).

24. Finucane, H.K. *et al*. Partitioning heritability by functional annotation using genome-wide association summary statistics. *Nat. Genet.* **47**, 1228–1235 (2015).

25. Cross-Disorder Group of the Psychiatric Genomics Consortium. Identification of risk loci with shared effects on five major psychiatric disorders: a genome-wide analysis. *Lancet* **381**, 1371–1379 (2013).

26. Garnier, S. *et al*. Genome-wide haplotype analysis of cis expression quantitative trait loci in monocytes. *PLoS Genet.* **9**, e1003240 (2013).

27. Fairfax, B.P. *et al*. Innate immune activity conditions the effect of regulatory variants upon monocyte gene expression. *Science* **343**, 1246949 (2014).

28. Zhang, Y. *et al*. Purification and characterization of progenitor and mature human astrocytes reveals transcriptional and functional differences with mouse. *Neuron* **89**, 37–53 (2016).

29. Zhang, Y. *et al*. An RNA-sequencing transcriptome and splicing database of glia, neurons, and vascular cells of the cerebral cortex. *J. Neurosci.* **34**, 11929–11947 (2014).

30. Bennett, M.L. *et al*. New tools for studying microglia in the mouse and human CNS. *Proc. Natl. Acad. Sci. USA* **113**, E1738–E1746 (2016).

31. Giambartolomei, C. *et al*. Bayesian test for colocalisation between pairs of genetic association studies using summary statistics. *PLoS Genet.* **10**, e1004383 (2014).

32. Hikami, K. *et al*. Association of a functional polymorphism in the 3′-untranslated region of *SPI1* with systemic lupus erythematosus. *Arthritis Rheum.* **63**, 755–763 (2011).

33. Ward, L.D. & Kellis, M. HaploReg: a resource for exploring chromatin states, conservation, and regulatory motif alterations within sets of genetically linked variants. *Nucleic Acids Res.* **40**, D930–D934 (2012).

34. Pham, T.H. *et al*. Dynamic epigenetic enhancer signatures reveal key transcription factors associated with monocytic differentiation states. *Blood* **119**, e161–e171 (2012).

35. Steinberg, S. *et al*. Loss-of-function variants in *ABCA7* confer risk of Alzheimer's disease. *Nat. Genet.* **47**, 445–447 (2015).

36. Bernstein, B.E. *et al*.; ENCODE Project Consortium. An integrated encyclopedia of DNA elements in the human genome. *Nature* **489**, 57–74 (2012).

37. Sakai, K. *et al*. A neuronal *VLDLR* variant lacking the third complement-type repeat exhibits high capacity binding of apoE containing lipoproteins. *Brain Res.* **1276**, 11–21 (2009).

38. Bajari, T.M., Strasser, V., Nimpf, J. & Schneider, W.J. A model for modulation of leptin activity by association with clusterin. *FASEB J.* **17**, 1505–1507 (2003).

39. Speliotes, E.K. *et al*. Association analyses of 249,796 individuals reveal 18 new loci associated with body mass index. *Nat. Genet.* **42**, 937–948 (2010).

40. Strawbridge, R.J. *et al*. Genome-wide association identifies nine common variants associated with fasting proinsulin levels and provides new insights into the pathophysiology of type 2 diabetes. *Diabetes* **60**, 2624–2634 (2011).

41. Satoh, J., Asahina, N., Kitano, S. & Kino, Y. A comprehensive profile of ChIP-seq-based PU.1/Spi1 target genes in microglia. *Gene Regul. Syst. Bio.* **8**, 127–139 (2014).

42. Daniel, B. *et al*. The active enhancer network operated by liganded RXR supports angiogenic activity in macrophages. *Genes Dev.* **28**, 1562–1577 (2014).

43. McKercher, S.R. *et al*. Targeted disruption of the PU.1 gene results in multiple hematopoietic abnormalities. *EMBO J.* **15**, 5647–5658 (1996).

44. Beers, D.R. *et al*. Wild-type microglia extend survival in PU.1 knockout mice with familial amyotrophic lateral sclerosis. *Proc. Natl. Acad. Sci. USA* **103**, 16021–16026 (2006).

45. Mak, K.S., Funnell, A.P.W., Pearson, R.C.M. & Crossley, M. PU.1 and haematopoietic cell fate: dosage matters. *Int. J. Cell Biol.* **2011**, 808524 (2011).

46. Smith, A.M. *et al*. The transcription factor PU.1 is critical for viability and function of human brain microglia. *Glia* **61**, 929–942 (2013).

47. Butovsky, O. *et al*. Identification of a unique TGF-β-dependent molecular and functional signature in microglia. *Nat. Neurosci.* **17**, 131–143 (2014).

48. Wang, Y. *et al*. IL-34 is a tissue-restricted ligand of CSF1R required for the development of Langerhans cells and microglia. *Nat. Immunol.* **13**, 753–760 (2012).

49. Dagher, N.N. *et al*. Colony-stimulating factor 1 receptor inhibition prevents microglial plaque association and improves cognition in 3xTg-AD mice. *J. Neuroinflammation* **12**, 139 (2015).

50. Alpérovitch, A. *et al*.; 3C Study Group. Vascular factors and risk of dementia: design of the Three-City Study and baseline characteristics of the study population. *Neuroepidemiology* **22**, 316–325 (2003).

51. Dreses-Werringloer, U. *et al*. A polymorphism in *CALHM1* influences Ca2+ homeostasis, Abeta levels, and Alzheimer's disease risk. *Cell* **133**, 1149–1161 (2008).

52. Lopez, O.L. *et al*. Evaluation of dementia in the cardiovascular health cognition study. *Neuroepidemiology* **22**, 1–12 (2003).

53. Dawber, T.R. & Kannel, W.B. The Framingham study. An epidemiological approach to coronary heart disease. *Circulation* **34**, 553–555 (1966).

54. Feinleib, M., Kannel, W.B., Garrison, R.J., McNamara, P.M. & Castelli, W.P. The Framingham offspring study. Design and preliminary data. *Prev. Med.* **4**, 518–525 (1975).

55. Splansky, G.L. *et al*. The third generation cohort of the National Heart, Lung, and Blood Institute's Framingham heart study: design, recruitment, and initial examination. *Am. J. Epidemiol.* **165**, 1328–1335 (2007).

56. Beiser, A., D'Agostino, R.B. Sr., Seshadri, S., Sullivan, L.M. & Wolf, P.A. Computing estimates of incidence, including lifetime risk: Alzheimer's disease in the Framingham study. the Practical Incidence Estimators (PIE) macro. *Stat. Med.* **19**, 1495–1522 (2000).

57. Bachman, D.L. *et al*. Incidence of dementia and probable Alzheimer's disease in a general population: the Framingham Study. *Neurology* **43**, 515–519 (1993).

58. Farmer, M.E. *et al*. Neuropsychological test performance in Framingham: a descriptive study. *Psychol. Rep.* **60**, 1023–1040 (1987).

59. DeCarli, C. *et al*. Measures of brain morphology and infarction in the Framingham heart study: establishing what is normal. *Neurobiol. Aging* **26**, 491–510 (2005).

60. Au, R. *et al*. New norms for a new generation: cognitive performance in the framingham offspring cohort. *Exp. Aging Res.* **30**, 333–358 (2004).

61. Seshadri, S. & Wolf, P.A. Lifetime risk of stroke and dementia: current concepts, and estimates from the Framingham Study. *Lancet Neurol.* **6**, 1106–1114 (2007).

62. Hofman, A. *et al*. The Rotterdam Study: 2014 objectives and design update. *Eur. J. Epidemiol.* **28**, 889–926 (2013).

63. Fagan, A.M. *et al*. Inverse relation between *in vivo* amyloid imaging load and cerebrospinal fluid Abeta42 in humans. *Ann. Neurol.* **59**, 512–519 (2006).

64. Peskind, E., Nordberg, A., Darreh-Shori, T. & Soininen, H. Safety of lumbar puncture procedures in patients with Alzheimer's disease. *Curr. Alzheimer Res.* **6**, 290–292 (2009).

65. Grimmer, T. *et al*. Beta amyloid in Alzheimer's disease: increased deposition in brain is reflected in reduced concentration in cerebrospinal fluid. *Biol. Psychiatry* **65**, 927–934 (2009).

66. Blennow, K., Hampel, H., Weiner, M. & Zetterberg, H. Cerebrospinal fluid and plasma biomarkers in Alzheimer disease. *Nat. Rev. Neurol.* **6**, 131–144 (2010).

67. Willer, C.J., Li, Y. & Abecasis, G.R. METAL: fast and efficient meta-analysis of genomewide association scans. *Bioinformatics* **26**, 2190–2191 (2010).

68. Peskind, E.R. *et al*. Age and apolipoprotein *E*4* allele effects on cerebrospinal fluid beta-amyloid 42 in adults with normal cognition. *Arch. Neurol.* **63**, 936–939 (2006).

69. Purcell, S. *et al*. PLINK: a tool set for whole-genome association and population-based linkage analyses. *Am. J. Hum. Genet.* **81**, 559–575 (2007).

70. Howie, B.N., Donnelly, P. & Marchini, J. A flexible and accurate genotype imputation method for the next generation of genome-wide association studies. *PLoS Genet.* **5**, e1000529 (2009).

71. Cox, D.R. Regression Models and Life-Tables. *J. R. Stat. Soc. B.* **34**, 187–220 (1972).

72. Prentice, R.L. & Breslow, N.E. Retrospective studies and failure time models. *Biometrika* **65**, 153–158 (1978).

73. van der Net, J.B. *et al*. Cox proportional hazards models have more statistical power than logistic regression models in cross-sectional

genetic association studies. *Eur. J. Hum. Genet.* **16**, 1111–1116 (2008).

74. Pruim, R.J. *et al*. LocusZoom: regional visualization of genome-wide association scan results. *Bioinformatics* **26**, 2336–2337 (2010).

75. Zhou, X. *et al*. Exploring long-range genome interactions using the WashU Epigenome Browser. *Nat. Methods* **10**, 375–376 (2013).

76. Griffon, A. *et al*. Integrative analysis of public ChIP-seq experiments reveals a complex multi-cell regulatory landscape. *Nucleic Acids Res.* **43**, e27 (2015).

77. Sloan, C.A. *et al*. ENCODE data at the ENCODE portal. *Nucleic Acids Res.* **44**, D726–D732 (2016).

78. Roe, J.S., Mercan, F., Rivera, K., Pappin, D.J. & Vakoc, C.R. BET bromodomain inhibition suppresses the function of hematopoietic transcription factors in acute myeloid leukemia. *Mol. Cell* **58**, 1028–1039 (2015).

79. Wang, X. & Seed, B. A PCR primer bank for quantitative gene expression analysis. *Nucleic Acids Res.* **31**, e154 (2003).

Download references

Acknowledgments

We thank the patients, control subjects and their family members for participating in and supporting the research projects included in this study. We thank M. Diamond (UT Southwestern Medical Center) for the BV2 cell line and the Flow Cytometry CORE at the Icahn School of Medicine at Mount Sinai Hospital.

IGAP: This study incorporated imputed summary results from the GERAD1 genome-wide association study. GERAD was supported by the Wellcome Trust, the MRC, Alzheimer's Research UK (ARUK) and the Welsh government. ADGC and CHARGE were supported by the US National Institutes of Health, National Institute on Aging (NIH-NIA), including grants U01 AG032984 and R01 AG033193. CHARGE was also supported by Erasmus Medical Center and Erasmus University.

Cardiff University was supported by the Wellcome Trust, Medical Research Council (MRC), Alzheimer's Research UK (ARUK) and the Welsh Assembly Government. Cambridge University and Kings College London acknowledge support from the MRC. ARUK supported sample collections at the South West Dementia Bank and the Universities of Nottingham, Manchester and Belfast. The Belfast group acknowledges support from the Alzheimer′s Society, Ulster Garden Villages, N. Ireland R&D Office and the Royal College of Physicians/Dunhill Medical Trust. The MRC and Mercer's Institute for Research on Aging supported the Trinity College group. The South West Dementia Brain Bank acknowledges support from Bristol Research into Alzheimer's and Care of the Elderly. The Charles Wolfson Charitable Trust supported the OPTIMA group. Washington University was funded by NIH grants, Barnes Jewish Foundation and by the Charles and Joanne Knight Alzheimer's Research Initiative. Patient recruitment for the MRC Prion Unit/UCL Department of Neurodegenerative Disease collection was supported by the UCLH/UCL Biomedical Centre and NIHR Queen Square Dementia Biomedical Research Unit. LASER-AD was funded by Lundbeck SA. The Bonn group was supported by the German Federal Ministry of Education and Research (BMBF), Competence Network Dementia and Competence Network Degenerative Dementia and by the Alfried Krupp von Bohlen und Halbach-Stiftung. The GERAD Consortium also used samples ascertained by the NIMH AD Genetics Initiative.

The KORA F4 studies were financed by Helmholtz Zentrum München; German Research Center for Environmental Health; BMBF; German National Genome Research Network and the Munich Center of Health Sciences. The Heinz Nixdorf Recall cohort was funded by the Heinz Nixdorf Foundation (Dr. jur. G.Schmidt, Chairman) and BMBF. Coriell Cell Repositories is supported by NINDS and the Intramural Research Program of the National Institute on Aging. We acknowledge use of genotype data from the 1958 Birth Cohort collection, funded by the MRC and the Wellcome Trust, which was genotyped by the Wellcome Trust Case Control Consortium and the Type-1 Diabetes Genetics Consortium, sponsored by the National Institute of Diabetes and Digestive and Kidney Diseases, National Institute of Allergy and Infectious Diseases, National Human Genome Research Institute, National Institute of Child Health and Human Development and Juvenile Diabetes Research Foundation International.

ADNI: Data collection and sharing for this project was funded by the Alzheimer′s Disease Neuroimaging Initiative (National Institutes of Health Grant U01 AG024904) and DOD ADNI (Department of Defense award number W81XWH-12-2-0012). ADNI is funded by the National

Institute on Aging and the National Institute of Biomedical Imaging and Bioengineering and through generous contributions from the following: AbbVie, Alzheimer's Association; Alzheimer's Drug Discovery Foundation; Araclon Biotech; BioClinica, Inc.; Biogen; Bristol-Myers Squibb Company; CereSpir, Inc.; Eisai Inc.; Elan Pharmaceuticals, Inc.; Eli Lilly and Company; EuroImmun; F. Hoffmann-La Roche Ltd and its affiliated company, Genentech, Inc.; Fujirebio; GE Healthcare; IXICO Ltd.; Janssen Alzheimer Immunotherapy Research & Development, LLC.; Johnson & Johnson Pharmaceutical Research & Development LLC.; Lumosity; Lundbeck; Merck & Co., Inc.; Meso Scale Diagnostics, LLC.; NeuroRx Research; Neurotrack Technologies; Novartis Pharmaceuticals Corporation; Pfizer Inc.; Piramal Imaging; Servier; Takeda Pharmaceutical Company; and Transition Therapeutics. The Canadian Institutes of Health Research is providing funds to support ADNI clinical sites in Canada. Private sector contributions are facilitated by the Foundation for the National Institutes of Health (https://fnih.org/). The grantee organization is the Northern California Institute for Research and Education, and the study is coordinated by the Alzheimer's Disease Cooperative Study at the University of California, San Diego. ADNI data are disseminated by the Laboratory for Neuro Imaging at the University of Southern California.

We thank the Cardiogenics (European Project reference LSHM-CT-2006-037593) project for providing summary statistics for the *cis*-eQTL-based analyses. We also thank the ENCODE Consortium and R. Myers' lab (HAIB) for providing ChIP-seq datasets.

This work was supported by grants from the National Institutes of Health (U01 AG049508, R01-AG035083 and RF-AG054011 (to A.M.G.) and R01-AG044546 and RF1AG053303 (to C.C.)), the JPB Foundation (to A.M.G.) and F Prime (to A.M.G.). The recruitment and clinical characterization of research participants at Washington University were supported by NIH P50 AG05681, P01 AG03991 and P01 AG026276. Kuan-lin Huang received fellowship funding in part from the Ministry of Education in Taiwan and the Lucille P. Markey Special Emphasis Pathway in Human Pathobiology. Ke Hao is partially supported by the National Natural Science Foundation of China (Grant Nos. 21477087 and 91643201) and by the Ministry of Science and Technology of China (Grant No. 2016YFC0206507). This work was supported by access to equipment made possible by the Hope Center for Neurological Disorders and the Departments of Neurology and Psychiatry at Washington University School of Medicine.

Author information

These authors contributed equally to this work.
Kuan-lin Huang & Edoardo Marcora

Affiliations

Department of Medicine and McDonnell Genome Institute, Washington University in St. Louis, Saint Louis, Missouri, USA.
Kuan-lin Huang

Department of Genetics and Genomic Sciences, Icahn School of Medicine at Mount Sinai, New York,New York, USA.
Edoardo Marcora, Antonio F Di Narzo, Manav Kapoor, Andrew McKenzie, Towfique Raj, Bin Zhang, Ke Hao & Alison M Goate

Ronald M. Loeb Center for Alzheimer's Disease, Department of Neuroscience, Icahn School of Medicine at Mount Sinai, New York,New York, USA.
Edoardo Marcora, Anna A Pimenova, Manav Kapoor, Sarah Bertelsen, Towfique Raj, Alan E Renton & Alison M Goate

Department of Genetics, Yale University School of Medicine, New Haven, Connecticut, USA.
Sheng Chih Jin

Department of Psychiatry, Washington University in St. Louis, Saint Louis, Missouri, USA.
Oscar Harari, Yuetiva Deming, John Budde, Jorge L Del-Aguila, Maria Victoria Fernandez, Laura Ibañez & Carlos Cruchaga

Wellcome Trust Centre for Human Genetics, Nuffield Department of Medicine, University of Oxford, Oxford, UK.
Benjamin P Fairfax

Department of Genetics, Washington University in St. Louis, Saint Louis, Missouri, USA.
Jake Czajkowski & Ingrid Borecki

Department of Neurology, Boston University School of Medicine, Boston, Massachussets, USA.
Vincent Chouraki & Sudha Seshadri

Inserm, U1167, RID-AGE –Risk factors and molecular determinants of aging-related diseases, Lille, France.
Benjamin Grenier-Boley, Céline Bellenguez, Jean Charles Lambert & Philippe Amouyel

Univ. Lille - Excellence laboratory Labex DISTALZ, Lille, France.
Benjamin Grenier-Boley, Céline Bellenguez, Jean Charles Lambert & Philippe Amouyel

Institut Pasteur de Lille, Lille, France.
Benjamin Grenier-Boley, Céline Bellenguez, Jean Charles Lambert & Philippe Amouyel

Icelandic Heart Association, Faculty of Medicine, University of Iceland, Reykjavik, Iceland.
Albert Smith

Department of Epidemiology, University of Washington, Seattle, Washington, USA.
Annette Fitzpatrick

Department of Medicine, University of Washington, Seattle, Washington, USA.
Joshua C Bis

Department of Biostatistics, Boston University School of Public Health, Boston, Massachussetts, USA.
Anita DeStefano & Lindsay A Farrer

Department of Epidemiology, Erasmus University Medical Center, Rotterdam, the Netherlands.
Hieab H H Adams, M Arfan Ikram, Sven van der Lee & Cornelia van Duijn

Psychological Medicine and Clinical Neurosciences, Medical Research Council (MRC) Centre for Neuropsychiatric Genetics and Genomics, Cardiff University, Cardiff, UK.
Rebecca Sims, Valentina Escott-Price & Julie Williams

Taub Institute on Alzheimer's Disease and the Aging Brain, Gertrude H. Sergievsky Center, and Department of Neurology, Columbia University, New York,New York, USA.
Richard Mayeux

Department of Epidemiology and Biostatistics, Case Western Reserve University, Cleveland, Ohio, USA.
Jonathan L Haines

Department of Ophthalmology, Boston University School of Medicine, Boston, Massachussets, USA.
Lindsay A Farrer

Department of Epidemiology, Boston University School of Public Health, Boston, Massachussetts, USA.
Lindsay A Farrer

The John P. Hussman Institute for Human Genomics, University of Miami, Miami, Florida, USA.
Lindsay A Farrer & Margaret A Pericak-Vance

Macdonald Foundation Department of Human Genetics, University of Miami, Miami, Florida, USA.
Margaret A Pericak-Vance

Laboratory of Epidemiology and Population Sciences, National Institute on Aging, Bethesda, Maryland, USA.
Lenore Launer

Centre Hospitalier Universitaire de Lille, U1167, Lille, France.
Philippe Amouyel

Department of Pathology and Laboratory Medicine, University of Pennsylvania Perelman School of Medicine, Philadelphia, Pennsylvania, USA.
Gerard D Schellenberg

Department of Biology, Brigham Young University, Provo, Utah, USA.
John S K Kauwe

Consortia

The International Genomics of Alzheimer's Project

A full list of members and affiliations appears in the Supplementary Note.

The Alzheimer's Disease Neuroimaging Initiative

A full list of members and affiliations appears in the Supplementary Note.

Contributions

A.M.G., E.M. and K.-L.H. conceived and designed the experiments. K.-L.H., S.C.J., O.H., A.D., M.K., J.C., J.C.L., V.C., C.B., B.G.-B., Y.D., A.M., T.R., A.E.R., J.L.D.-A., M.V.F, L.I., B.Z., I.B., C.C. and E.M. performed data analysis. A.A.P. performed phagocytosis assays, western blotting and qPCR validation. S.B., B.P.F., J.B., R.S., V.E.-P., R.M., J.L.H., L.A.F., M.A.P.-V., S.S., J.W., P.A., G.D.S., J.S.K.K., K.H. and C.C. provided and processed the data. A.M.G. supervised data analysis and functional experiments. K.-L.H., A.A.P., E.M. and A.M.G. wrote and edited the manuscript. All authors read and approved the manuscript.

Competing financial interests

A.M.G. is on the scientific advisory board for Denali Therapeutics and has served as a consultant for AbbVie and Cognition Therapeutics.

Corresponding author

Correspondence to: Alison M Goate

Supplementary information

Supplementary Figures

1. Supplementary Figure 1: Result and quality control analysis of the IGAP AD-survival meta-analysis. (32 KB)
   (a) Manhattan plot and QQ-plot of the GWAS. The final meta-analysis showed little evidence of genomic inflation (λ = 1.026). (b) The average standard error versus the number of cohorts with consistent directionalities of effect sizes.

2. Supplementary Figure 2: Kaplan-Meier plots of AAOS associations. (30 KB)
   Kaplan-Meier plots of survival analysis associations in the ADGC cohort of (a) rs1057233, (b) rs10919252, (c) rs567075, (d) rs7867518, (e) rs7930318, (f) rs4803758.

3. Supplementary Figure 3: Forest plots of AAOS associations. (39 KB)
   Forest plots of survival analysis associations across IGAP cohorts of (a) rs1057233, (b) rs10919252, (c) rs567075, (d) rs7867518, (e) rs7930318, (f) rs4803758.

4. Supplementary Figure 4: Cell-type-specific expression of eQTL-associated genes in brain. (79 KB)
   Cell-type specific expression of *MS4A4A* (no mouse homolog available), *SPI1*, *MYBPC3*, *MS4A6A* and *SELL* in human and mouse brains based on the brain RNA-Seq database.

5. Supplementary Figure 5: Linkage disequilibrium (LD) plot of SNPs of interest in the *SPI1* (*CELF1*) locus. (48 KB)

6. Supplementary Figure 6: SMR plots showing the associations at the *SPI1* locus. (78 KB)
   SMR plots showing the associations at the *SPI1/CELF1* locus from AAOS GWAS and eQTLs in (a) monocytes and (b) macrophages.

7. Supplementary Figure 7: *SPI1* (PU.1) ChIP-seq binding sites and other epigenetic signatures at AD-associated loci in human CD14$^+$ monocytes. (97 KB)
   PU.1 binding sites, DNase I hypersensitive sites, histone modifications, and chromatin states at the locus of (**a**) *ABCA7*, (**b**) *APOE*, (**c**) *BIN1*, (**d**) *SPI1*, (**e**) *PICALM*, and (f) *TYROBP*.

8. Supplementary Figure 8: Analysis of phagocytosis in BV2 microglial cells. (314 KB)
   (**a**) Flow cytometry histograms of BV2 cells transfected with pcDNA3 (pcDNA) or pcDNA3-FLAG-PU.1 (FLAG-PU.1) with pCMV-GFP for overexpression and scrambled shRNA (shSCR) or shRNA targeting PU.1 (shA, shB and shD) in pGFP-V-RS vector for knock-down of PU.1 after 3 hours of incubation with pHrodo-labeled zymosan. Cells were gated on GFP$^+$ population. (**b**) Flow cytometry analysis of the number of gated cells in **a** presented as mean ± s.d., pcDNA 67.03 ± 6.883, pcDNA + 1 μM Cyt 15.64 ± 16.24, FLAG-PU.1 82.71 ± 4.74, shSCR 77.17 ± 3.115, shA 48.63 ± 2.285, shB 28.92 ± 2.495, shD 22.76 ± 1.595. pcDNA vs pcDNA + 1 μM Cyt $P < 0.0001$, pcDNA vs FLAG-PU.1 $P = 0.0306$, shSCR vs shA $P = 0.0002$, shSCR vs shB $P < 0.0001$, shSCR vs shD $P < 0.0001$. $F(6,13) = 58.68$, $n = 3$. (**c**) Flow cytometry analysis of the geometric mean fluorescent pHrodo intensity in **a** presented as mean ± s.d., pcDNA 10952 ± 2206, pcDNA + 1 μM Cyt 1533 ± 47, FLAG-PU.1 15226 ± 2701, shSCR 13129 ± 4617, shA 9937 ± 2168, shB 8872 ± 2019, shD 8754 ± 1856. pcDNA vs pcDNA + 1 μM Cyt $P = 0.0092$. $F(6,13) = 6.228$, $n = 3$. (**d**) Flow cytometry histograms of BV2 cells transfected as in (**a**) and gated on GFP- populations. (**e**) Flow cytometry analysis of number of gated cells in **d** presented as mean ± s.d., pcDNA 63.92 ± 6.575, pcDNA + 1 μM Cyt 14.21 ± 13.66, FLAG-PU.1 67.54 ± 4.826, shSCR 68.31 ± 5.784, shA 67.27 ± 4.144, shB 65.19 ± 4.268, shD 60.3 ± 2.181. pcDNA vs pcDNA + 1 μM Cyt $P < 0.0001$. $F(6,13) = 22.53$, $n = 3$. (**f**) Flow cytometry analysis of geometric mean fluorescent pHrodo intensity in **d** presented as mean ± s.d., pcDNA 9186 ± 2863, pcDNA + 1 μM Cyt 1545 ± 147, FLAG-PU.1 9931 ± 2458, shSCR 9849 ± 3012, shA 10903 ± 2949, shB 10912 ± 2494, shD 10934 ± 2685. pcDNA vs pcDNA + 1 μM Cyt $P = 0.0367$. $F(6,13) = 3.473$, $n = 3$. (**g**) Phagocytic index of BV2 GFP$^-$ cells analyzed in (**e**) and (**f**) presented as mean ± s.d., pcDNA 0.5954 ± 0.2223, pcDNA + 1 μM Cyt 0.0209 ± 0.0189, FLAG-PU.1 0.6745 ± 0.188, shSCR 0.6765 ± 0.2274, shA 0.7382 ± 0.2255, shB 0.7131 ± 0.1742, shD 0.6612 ± 0.1748. pcDNA vs pcDNA + 1 μM Cyt $P = 0.0331$. $F(6,13) = 3.53$, $n = 3$. Cytochalasin D (Cyt) treatment was used as a negative control. * $P < 0.05$, ** $P < 0.01$, *** $P < 0.001$, one-way ANOVA with Sidak's *post hoc* multiple comparisons test between selected groups.

9. Supplementary Figure 9: Expression levels of genes related to phagocytosis that were not affected by altered *Spi1* expression. (61 KB)
   BV2 cells were transiently transfected with pcDNA3-FLAG-PU.1 and pCMV-GFP or pGFP-V-RS-shB against PU.1. pcDNA3 and pGFP-V-RS-shSCR were used as controls. RNA was extracted from sorted GFP$^+$ cells and used for qPCR validation of expression levels for genes of interest. Values are presented as mean ± s.d., $n = 4$ samples collected independently.

PDF files

1. Supplementary Text and Figures (1,360 KB)
   Supplementary Figures 1–9.

2. Supplementary Methods Checklist (201 KB)

3. Supplementary Note (70 KB)

Excel files

1. Supplementary Table 1 (16 KB)
   Quality control of the age-at-onset survival GWAS. The number of filtered SNPs and samples are shown for each of the 7 cohort included for the IGAP meta-analysis. Additionally, the Schoenfeld P values were recorded for each of the 22 top AAOS GWAS SNPs across the 7 IGAP cohorts, and the covariates in Cox models for the ADGC and GERAD cohorts.

2. Supplementary Table 2 (12 KB)
   Association results from the previous IGAP logistic regression and the matching cohort logistic regression of the 22 top AD-associated SNPs in AAOS GWAS.

3. Supplementary Table 3 (488 KB)
   The 22 top SNPs significantly associated with age-at-onset defined survival in AD and their tag SNPs ($R^2 \geq 0.8$).

4. Supplementary Table 4 (8 KB)
   Significant cis-eQTL associations between the 22 survival-associated SNPs across 10 brain regions in the BRAINEAC dataset.
   Bonferroni-corrected threshold: P=0.05/292,000 probes = 1.7×10^{-7}.

5. Supplementary Table 5 (74 KB)
   Significant cis-eQTL associations between the 22 survival-associated SNPs across tissues in the GTEx dataset.

6. Supplementary Table 6 (119 KB)
   LD score regression analysis results for IGAP AD and PGC SCZ GWAS SNP heritability partitioned using 220 human cell types (CT, and 10 cell type groups, CTG)-specific functional annotations as described by Finucane et al.

7. Supplementary Table 7 (8 KB)
   Replication of monocyte/macrophage cis-eQTL associations in CD14+ human monocytes from 432 individuals of European ancestry.
   Bonferroni-corrected threshold: P=0.05/15421 probes = 3.24×10^{-6}.

8. Supplementary Table 8 (90 KB)
   Coloc analysis results for the *SPI1/CELF1*, *MS4A* and *SELL* loci, using AAOS GWAS SNPs and Cardiogenics monocyte (MC) or macrophage (MP) cis-eQTL datasets.
   Estimated posterior probabilities for the following mutually exclusive hypotheses are shown in bold when surpassing the threshold PP ≥ 0.8: H0, neither trait has a genetic association in the region; H1: only trait 1 (cis-eQTL) has a genetic association in the region; H2: only trait 2 (GWAS) has a genetic association in the region; H3: both traits are associated, but with different causal variants; H4: both traits are associated and share a single causal variant.

9. Supplementary Table 9 (11 KB)
   Conditional analysis of monocyte/macrophage *SPI1* eQTL associations of 6 SNPs of interest: rs1057233, rs10838698, rs10838699, rs7928163, rs1377416, and rs10838725.
   Bonferroni-corrected threshold: P=0.05/6 SNPs = 0.00833.

10. Supplementary Table 10 (86 KB)
    SMR/HEIDI analysis results for 6 SNPs of interest in the *SPI1/CELF1* locus: rs1057233, rs10838698, rs10838699, rs7928163, rs1377416 and rs10838725, using AAOS GWAS SNPs and Cardiogenics monocyte (MC) or macrophage (MP) cis-eQTL datasets.
    Bonferroni-corrected threshold: SMR P=0.05/(6 SNPs x 17 probes) = 0.00049 [green cells]. A nominal significance threshold P ≥ 0.05 [red cells] is used for the HEIDI test as motivated by Zhu et al. Only probes with nominally significant SMR P are shown.

11. Supplementary Table 11 (46 KB)
    AD-associated genes expressed in human brain myeloid cells with nearby *SPI1* (PU.1) binding sites in human blood myeloid cells.

12. Supplementary Table 12 (13 KB)
    LD score regression analysis results for IGAP AD and PGC SCZ GWAS SNP heritability partitioned using *SPI1* (PU.1) ChIP-Seq binding sites in human monocytes and macrophages, as well as SPI1 (PU.1) and POLR2AphosphoS5 ChIP-Seq

binding sites in human HL60 cells.

13. Supplementary Table 13 (12 KB)
    Genes regulated in BV2 microglial cells with differential expression of *Spi1*.

14. Supplementary Table 14 (14 KB)
    Primers used for qPCR validation of gene expression in BV2 microglial cells.

Nature Neuroscience ISSN 1097-6256 EISSN 1546-1726